COMPUTATIONAL FLUID DYNAMICS STUDY OF NASAL CAVITY MODEL

VIZY NAZIRA BINTI RIAZUDDIN

UNIVERSITI SAINS MALAYSIA

2011

COMPUTATIONAL FLUID DYNAMICS STUDY OF NASAL CAVITY MODEL

by

VIZY NAZIRA BINTI RIAZUDDIN

Thesis submitted in fulfillment of the requirements

for the degree of

Master of Science

UNIVERSITI SAINS MALAYSIA

July 2011

ACKNOWLEDGEMENT

Alhamdulillah. Thanks and glory be to Allah (SWT) alone, for giving me this opportunity, strength and patience to complete my dissertation finally, after all the challenges and difficulties.

First and foremost, I would like to express my deepest appreciation to my supervisor; Dr. Kamarul Arifin bin Ahmad, whose encouragement, guidance and support from the very beginning which enabled me to develop the understanding of the subject.

My sincere thanks to Prof. Dr. Zulkifly Abdullah, Prof. Dr. Ibrahim Lutfi Shuaib, Dr. Rushdan Ismail, Assoc. Prof. Dr. Suzina Sheikh Abdul Hamid, and Mr. Mohamad Zihad Mahmud for their continuous thoughtful advice in bringing this research works to fruition. I would like to acknowledge my research colleague, Mr. Mohammed Zubair for his invaluable assistance and support throughout the entire research. I would like to thank all my colleagues for the joyful memories throughout the research.

Special thanks to Mohd Shahadan Mohd Suan, Khairunisa Zulkurnain and my parents, Riazuddin Ahmad Ali and Norizan Osman for their support and encouragement that enabled me to endure the hardship of my academic career.

TABLE OF CONTENTS

CHAPTER 4 – RESULTS AND DISCUSSION

LIST OF TABLES

LIST OF FIGURES

LIST OF ABBREVIATIONS

3D	Three Dimensional
AMDI	Advanced Medical and Dental Institute
AR	Atrophic Rhinitis
AAR	Active Anterior Rhinometry
CAD	Computational Aid Design
CAT	Computerized Axial Tomography
CFD	Computational Fluid Dynamics
CPU	Central Processing Unit
CT	Computed Tomography
DSE	Digitized Shape Editor
EIM	Eddy Interaction Model
ENT	Ear, Nose and Throat
HU	Hounsfield Units
IBM	International Business Machines
IGES	Initial Graphics Exchange Specification
LES	Large Eddy Simulation

MRI	Magnetic Resonance Imaging
NAR	Nasal Airway Resistance
OSA	Obstructive Sleep Apnea
RAM	Random-Access Memory
RANS	Reynolds Average Navier Stoke
SST	Shear Stress Transport Model
STP	STEP File/Standard for the Exchange of Product File

LIST OF SYMBOLS

ROMAN SYMBOLS

d	Diameter of the nasal inlet
k	Turbulent kinetic energy
Re	Reynolds number
R	Resistance
S_Φ	The source term of Φ
t	Time
u	Velocity vector
V	Velocity of the flow
y	The distance to the wall
u_τ	Friction velocity
v	Kinematic viscosity of the fluid flow

GREEK SYMBOLS

Γ	Diffusion coefficient
∂	Partial differential equation
Φ	General scalar
ε	Dissipated rate of k
ω	Specific rate of dissipation of k
ρ	Fluid density
μ	Dynamic viscosity of the air

ΔP Pressure drop

SUBSCRIPTS

vel Velocity

SUPERSCRIPT

+ Variable expressed in wall units

KAJIAN PENGKOMPUTERAN DINAMIK BENDALIR TERHADAP MODEL RONGGA HIDUNG

ABSTRAK

Pemahaman terhadap sifat-sifat aliran udara di dalam rongga hidung adalah sangat penting dalam menentukan fisiologi hidung dan dalam membantu diagnosis penyakit yang berkaitan dengan hidung. Setiap manusia mempunyai anatomi rongga hidung yang berbeza. Perubahan dari segi morfologi fisiologi hidung manusia juga telah ditentukan berdasarkan jantina. Terdahulu, tiada sebarang kajian pemodelan numerik yang khusus telah dilakukan bagi membanding serta memastikan pengaruh jantina terhadap pembolehubah aliran dalam rongga hidung. Tambahan pula, pelbagai langkah pemudahan yang berkaitan dengan perubahan postur badan dan penetapan keadaan persempadanan telah diambil bagi melaksanakan pemodelan numerik sehingga mempengaruhi hasil kajian pengaliran udara. Oleh itu, dalam kajian ini, permodelan rongga hidung dalam bentuk tiga dimensi telah dibangunkan dengan menggunakan imej tomografi milik individu perempuan Malaysia yang sihat. Sebuah kesinambungan keadaan mantap dan persamaan *Navier Stoke* telah diselesaikan dalam kedua-dua mekanisme inspirasi dan ekspirasi dengan tingkat aliran di antara 7.5-15 L/min sebagai laminar manakala nilai tingkat aliran di antara 20-40 L/min telah disimulasikan dalam keadaan aliran turbulen. Analisis menggunakan pengkomputeran dinamik bendalir (CFD) menghasilkan visualisasi yang sangat efektif terhadap ciri-ciri aliran di dalam rongga hidung. Nilai tegasan ricih maksimum pada bahagian dinding vestibule

meningkat melebihi 2000 % dengan penigkatan kadar aliran udara daripada 7.5 kepada 40 L/min. Perbandingan di antara mekanisme inspirasi dan ekspirasi serta pengaruh tahap pernafasan yang berbeza terhadap fungsi hidung telah dibentangkan. Anatomi rongga hidung yang kompleks ini telah dicipta bagi memenuhi keperluan fungsi fisiologi dalam membantu proses pernafasan secara normal. Hasil kajian ini telah mengenalpasti beberapa perbezaan anatomi dan fisiologi berdasarkan jantina. Penggunaan pengkomputeran dinamik bendalir telah membantu dalam memahami perbezaan yang wujud berdasarkan jantina yang tidak dapat diukur berdasarkan alat perubatan dan pemerhatian semata-mata. Pengaruh perubahan postur badan terhadap rongga hidung juga telah dikaji. Semasa perubahan posisi duduk kepada posisi baring, purata tekanan statik diperhatikan berubah pada nilai sekitar 0.3%. Perubahan arah graviti akibat daripada perubahan postur badan juga mempunyai pengaruh yang penting terhadap parameter aliran. Kebanyakan penyelidik menggunakan keadaan sempadan *plug flow* dalam menganalisis masalah yang berkaitan dengan aliran di dalam rongga hidung. Kajian ini telah mendedahkan kesilapan dalam menentukan keadaan sempadan dan mendapati wujudnya perbezaan yang jelas di antara hasil kajian yang telah diperolehi daripada kedua-dua kes. Pada bahagian injap rongga, rintangan pada *plug flow* adalah 0.311 Pa-min/L dan 0.147 Pa-min/L pada *pull flow*. Perubahan maksimum nilai rintangan yang berlaku pada bahagian vestibule adalah sebanyak 0.3578 Pa-min/L. Nilai purata halaju pada bahagian vestibule hidung adalah 1.4 m/s ketika *plug flow* dan 0.96 m/s ketika *pull flow*. Nilai purata halaju pada injap rongga pula adalah 1.6 m/s untuk *plug flow* dan 1.41 m/s untuk *pull flow*. Pendekatan yang lebih tepat bagi memodelkan mekanisme fisiologi inspirasi adalah dengan menggunakan model aliran *pull flow*.

COMPUTATIONAL FLUID DYNAMICS STUDY OF NASAL CAVITY MODEL

ABSTRACT

Understanding the properties of airflow in the nasal cavity is very important in determining the nasal physiology and in diagnosis of various anomalies associated with the nose. Inter-human anatomical variation for the nasal cavity exists and also differences on physiological morphology are observed based on gender. No specific numerical modeling studies have been carried out to compare and ascertain the effect of gender on flow variable inside the nasal cavity. Also numerical modeling involves various simplifications, for example the postural effect and appropriate boundary conditions which affect the outcome of the airflow studies. The present work involves development of three-dimensional nasal cavity models using computed tomographic images of healthy Malaysian females. A steady state continuity and Navier stoke equations were solved for both inspiratory and expiratory mechanism with flow rates ranging from 7.5 to 15 L/min as laminar and 20 to 40 L/min studies were simulated depicting turbulent flow conditions. Computational fluid dynamics (CFD) analysis provided effective visualization of the flow features inside the nasal cavity. The comparison between inspiratory and expiratory mechanism and the effect of different breathing rates on nasal function have been presented. The value of maximum wall shear stress at the vestibule region increased by more than 2000 % as the flow rate increased from 7.5 to 40 L/min. The complicated anatomy of the nasal cavity has been naturally designed to attain the physiological function desired to facilitate normal breathing. The

current study has identified certain gender based anatomical and physiological differences. The use of computational fluid dynamic has assisted in the understanding of these differences which could not be earlier quantified based on mere medical observation and measurement devices. The influence of postural changes in nasal cavity has also been investigated. Around 0.3% change in the average static pressure is observed while changing from sitting to supine position. The change in the direction of gravity due to change of posture significantly influences the flow parameters and hence should be considered in all future studies involving nasal flow. Most of the researchers employ plug flow boundary definitions to address the flow problems associated with nasal flow. This study has revealed the fallacy of such a definition and found significant differences in values obtained in either case. Comparative study of the pull flow model and the plug flow model has found significant variations highlighting the need for using the right boundary conditions. At the nasal valve, the resistance for plug flow was 0.311 Pa-min/L and for pull flow the value was 0.147 Pa-min/L. Maximum variation was noticed at the vestibule region with 0.3578 Pa-min/L. The average velocity for nasal vestibule and nasal valve is 1.4m/s and 1.6m/s for plug flow. Whereas, for pull flow case, the average velocity value in nasal vestibule and nasal valve region was observed to be around 0.96m/s and 1.41m/s respectively. A correct approach therefore to the numerical model is the pull flow model, which more directly represents the physiological inspiratory mechanism.

CHAPTER 1

INTRODUCTION

1.1 Research background

Nasal cavity is one of the most important components of human respiratory system. It provides the first line protection for lung by warming, humidifying and filtering the inspired air. The success of nasal function is highly dependent on the fluid dynamics characteristic of airflow through the nasal cavity. Better understanding of airflow characteristic in nasal cavity is essential to understand the physiology of nasal breathing.

Airflow through human nasal passages has been studied numerically and experimentally by a number of researchers (Wen *et al*., 2008; Mylavarapu *et al*., 2009; Segal *et al*., 2008; Weinhold *et al*., 2004). Also, several researchers have undertaken studies pertaining to airflow through nasal cavity using measuring devices such rhinomanometer and acoustic rhinomanometry (Hilberg *et al*., 1989, Sipilia *et al*., 1997, Jones *et al*., 1987, Shelton *et al*., 1992, Suzina *et al*., 2003). Rhinomanometry is used to measure the pressure required to produce airflow through the nasal airway and acoustic rhinomanometry is used to measure the cross sectional area of the airway at various nasal planes. However, measuring the precise velocity of airflow and evaluating the local nasal resistance in every portion of the nasal cavity have proven to be difficult (Ishikawa *et al*., 2006). The anatomical complexity of the nasal cavity makes it difficult for the measurement of nasal resistance. The small sizes of the nasal cavity and its narrow flow passage can cause perturbations in the airflow with any inserted probe.

Moreover, the reliability of the result obtained using this device depends on optimal cooperation from the subject, correct instructions from the investigator, and standardized techniques (Kjærgaard *et al*., 2009). There are reports of failure rates of between 25% and 50% in the subjects examined by rhinomanometry (Austin *et al*., 1994).

Due to the inherent limitations of these measuring devices, Computational Fluid Dynamics (CFD) has been proposed as a viable alternative. CFD which refers to use of numerical methods to solve the partial differential equation governing the flow of a fluid, is becoming an increasingly popular research tool in fluid dynamics. The non-invasive CFD modelling allows investigation of a wide variety of flow situations through human nasal cavities.

In order to investigate the physiology of human nasal function, many researchers have conducted numerical analysis to study the airflow profile in nasal respiration (Wen *et al*., 2008, Mylavarapu *et al*., 2009, Segal *et al*., 2008, Weinhold *et al*., 2004, Xiong *et al*., 2008, Croce *et al*., 2006, Garcia *et al*., 2007). However, most of the researchers employed male human subject in the determination of the nasal patency. Individual variation in nasal cavity anatomy existed and also differences on physiological morphology are observed based on gender. No specific numerical modelling studies have been carried out to compare and ascertain the effect of gender on flow variable inside the nasal cavity. Also CFD modelling involves various simplifications, for example the postural effect which affect the outcome of the airflow studies. Despite of the popularity of CFD in the study of nasal airflow, uncertainty still surrounds the appropriateness of the various assumptions made in CFD modelling, particularly with regards to the definition of boundary condition.

In the present study, inspiratory and expiratory steady airflow numerical simulations were performed using 3D nasal cavity model derived from computed tomography scan images. A comparative study is made of the female nasal cavity flow dynamics with that of the male nasal cavity as determined by other researchers. The effect of gravity on modelling nasal airflow and its effect on wall shear stress are also examined. Also plug and pull flow boundary conditions were compared to evaluate the effect of different boundary conditions on the flow parameters. Studies are carried out for various flow rates of 7.5 L/min, 10 L/min, 15 L/min, 20 L/min, 30 L/min and 40L/min suggesting various breathing rates.

1.2 Aims and Objectives

The overall objective of the present study is focused on the investigation of the airflow characteristic along the nasal airway during inspiration and expiration. The aims include the following objectives:

- To develop a three dimensional nasal cavity using the CT scans data.
- To carry out inspiratory steady state numerical simulation.
- To study the effect of different breathing conditions on the nasal physiology.
- To analyze the effect of different boundary conditions on the flow behavior.
- To investigate the effect of gravity and posture on flow properties inside the nasal cavity.

1.3 Scope of work

This research work was preliminarily performed by procuring CT scan images of human nasal cavity. The CT scan data was provided by Prof Ibrahim Lutfi Shuaib, a radiologist from Advanced Medical and Dental Institute (AMDI), Universiti Sains Malaysia. A normal nasal cavity of 39 year old Malaysian female was selected for the study case. The selected CT scan data was imported into MIMICs in order to process the scan images and to generate an accurate three-dimensional computational-aided design (CAD) model of the nasal airway. This was then followed by 3D surface geometry creation by using CATIA. The 3D nasal cavity model was imported into GAMBIT for mesh generation. Numerical simulation was further carried out by using FLUENT^{TM} and the result obtained was validated with previous published work.

1.4 Organization of the thesis

This thesis contains 5 chapters. The first chapter provides an introduction that reviews relevant research objectives, and related outlines of the purposes of this study. Chapter 2 presents an in-depth review of the background for this research. The chapter begins with an introduction to the anatomy and physiological function of the human nasal cavity and is followed by a review of previous studies related to the research. Chapter 3 presents the method used to construct a three dimensional human nasal cavity from CT scan and approach to CFD simulation. Chapter 4 presents the results obtained from the study cases. Finally, a summary of the results of the various studies and general conclusions reached, as well as suggestions for future work, are presented in Chapter 5.

CHAPTER 2

LITERATURE REVIEW

2.1 Overview

This chapter discusses nasal anatomy and physiology function of the human nasal cavity. The conventional method used in the measurement of the nasal cavity has been highlighted. A brief summary of the numerical modelling studies carried out by other researchers has been presented. The importance of gender comparison, effect of posture and the necessity for adopting the appropriate boundary condition in the numerical analysis of the nasal airflow has been literally evaluated.

2.2 Anatomy and physiology of the human nasal cavity

The anatomy and physiology of the human nasal cavity are presented in this section.

2.2.1 Nasal anatomy

The nose is the only external part of the respiratory system. It is made of bone and cartilage and fibro fatty tissues. As illustrated in Figure 2.11, the nasal cavity is divided into right and left cavities by a thin plate of bone and cartilage called the nasal septum. The nasal cavity lies above the hard plate. The hard portion of the palate forms the floor of the nasal cavity, separating it from the oral cavity below. The two openings in the nose called nostrils, allow air to enter or leave the body during breathing. Just beyond the external naris is a funnel shaped dilated region called the vestibule. The

narrow end of the funnel leads to a region referred to as the nasal valve. The nasal valve is the narrowest region of the nasal passage and has a special significance to the nasal function and nasal airflow pattern (Probst et al., 2006). At the end of the nasal valve the cross-sectional area of the airway increases, which mark the beginning of the main nasal passage (see Figure 2.1).

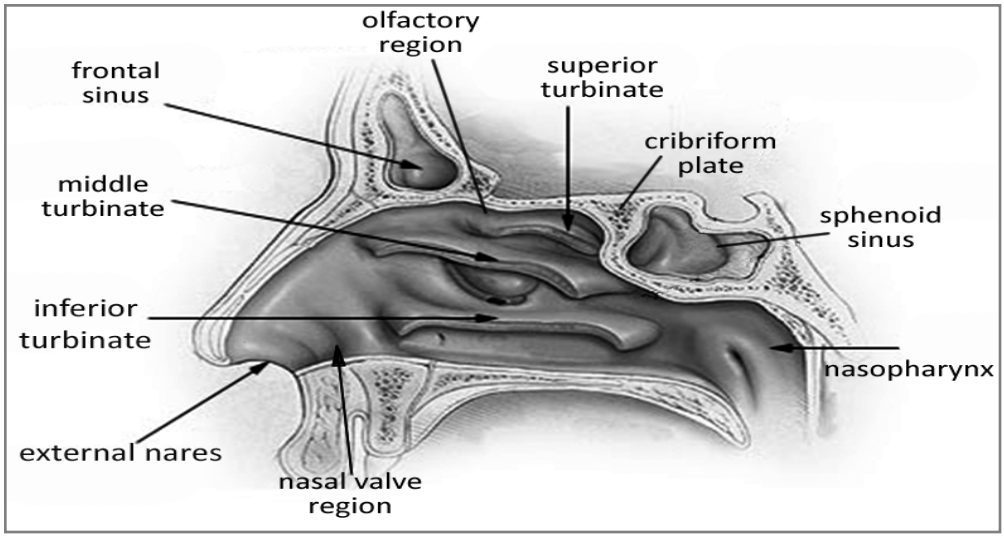

Figure 2.1: Diagram of the Nasal Cavity-reproduced from the Gray's anatomy of the human body, reproduced from Henry Gray, (1918)

On the lateral wall, there are three horizontal projections called turbinate or conchae, which divide the nasal cavity into three air passage. The three turbinates are named as inferior, middle and superior turbinates, according to their position and function (see Figure 2.2). The airway gap in between the turbinates and the central nasal septum walls is the meatus. The meatus are very narrow, normally being about 0.5-1mm. (Proctor and Andersen, 1982). At the posterior end of the main nasal passage, the turbinates and the septum end at the same point. The point at which the two nasal cavities merge into one and marks the beginning of the nasopharynx. At this point, the

cross section area of the airway is reduced and the path of the air-stream bends about 90º downwards towards the trachea (see Figure 2.3).

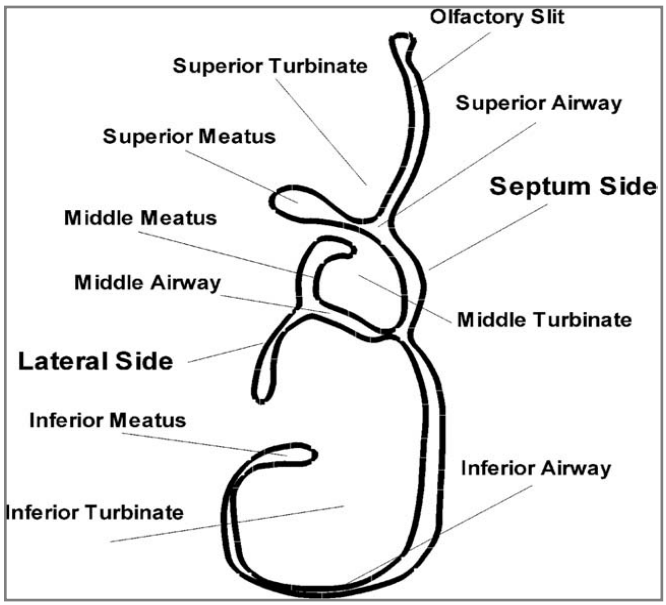

Figure 2.2: Coronal section of the main nose airway- reproduced from Zamankhan et al., (2006)

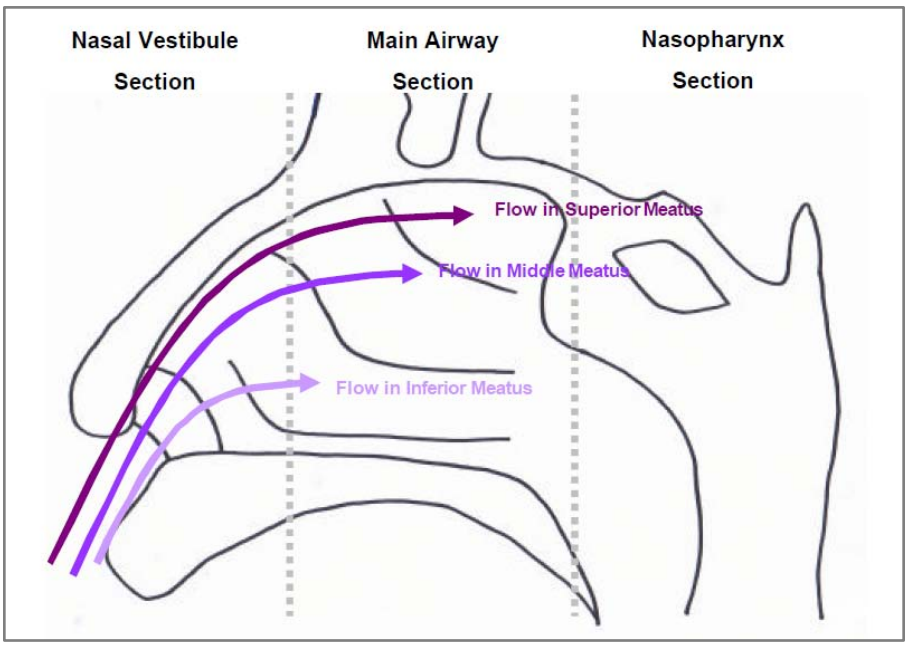

Figure 2.3: Simplified structure of the nasal cavity- reproduced from Tsui Wing Shum, (2009)

2.2.2 Nasal physiology

The human nose has two primary functions. The first is olfaction, the sense of smell. The second function is air-conditioning. Inspired air is conditioned by a combination of heating, humidification and filtering to provide the first line protection for the lung (Elad *et al*., 2008).

The nasal conchae help to slow down the passage air, causing it to swirl in the nasal cavity. The nasal cavity is lined by mucous membrane containing microscopic hairlike structures called cilia. The cells of the membrane produce mucus, a thick gooey liquid. The mucus moistens the air and traps any bacteria or particles of air pollution. Microscopic finger-like projections on the surface of the mucosal cells lining the nasal cavity called cilia. The cilia wave back and forth in rhythmic movement. Cilia will slowly propel the mucus backwards into the pharynx where it is swallowed. The nose is so effective that inspired air is cleared of all particulate matter larger than 6 microns-smaller than the size of a red blood cell.

The nose also acts as the organ of olfaction and has a specially adapted mucosal lining along its roof for this purpose. In order to stimulate the olfactory system (sense of smell), the odorant particles must interact with olfactory receptors located in the olfactory mucosa. Odorants must therefore be capable of being delivered to the olfactory region by inspired air and be able to dissolve sufficiently in the mucus covering the olfactory mucosa (Ishikawa *et al*., 2009).

2.3 Objective measurement methods

Objective measurement methods are the conventional tools utilized by medical practitioners to measure the physiology and anatomy of the nasal cavity. In this section, the main objective measurement methods are discussed namely rhinomanometry and acoustic rhinometry.

2.3.1 Rhinomanometry

Rhinomanometry is a tool which is used to measure nasal airway resistance by making a quantitative measurement of nasal flow and pressure. The European committee of standardization of Rhinomanometry has selected the formula $R = \Delta P/V$ at a fixed pressure of 150Pa; to facilitate comparison of results. (where R=resistance, ΔP=pressure drop, V is the velocity of flow). Rhinomanometry can be performed by anterior or posterior approaches. However this technique is time consuming and requires a great deal of patient cooperation, particularly difficult with children. It cannot be used in the presence of septal perforations and when one or both cavities are totally obstructed. It is affected by nasal cycle and errors as high as 25% are reported for repetitions within 15 minute (Hilberg *et al*., 1989). It cannot accurately assess a specific area of the nasal cavity. Rhinomanometry is time consuming, requires technical expertise, a high degree of subject cooperation and is impossible in subjects with severely congested nasal airways. There are reports of failure rates of between 25% and 50% in the subjects examined by rhinomanometry (Austin *et al*., 1994).

2.3.2 Acoustic Rhinometry (AR)

Acoustic Rhinometry analyses ultrasound waves reflected from the nasal cavity to calculate the cross sectional area at any point in the nasal cavity as well as the nasal volume. Acoustic rhinometry was first described for clinical use in 1989. The list of clinical problems that can be analyzed objectively with acoustic rhinometry has expanded to include turbinoplasty, sleep disorders, more types of cosmetic/reconstructive procedures, sinus surgery, vasomotor rhinitis, maxillofacial expansion procedures, and aspirin and methacholine challenge (Corey, 2006). Acoustic rhinometry is a tool that can aid in the assessment of nasal obstruction. The test is noninvasive, reliable, convenient, and easy to perform. Common clinical and practical uses of acoustic rhinometry for the rhinologic surgeon include assessment of “mixed" nasal blockage, documentation of nasal alar collapse, and preoperative planning for reduction rhinoplasty.

Acoustic rhinometry can also be used to document the positive effect of surgery on nasal airway obstruction (Devyani *et al*., 2004). However, AR may be unreliable due to artifacts (Tomkinson *et al*., 1998) & errors can occur in cross sectional area estimation (Tomkinson *et al*., 1995). Suzina *et al*., (2003) concluded that AAR is a sensitive but not a specific tool for the detection of abnormalities in NAR and it failed to relate to the symptom of nasal obstruction. There is a poor correlation between subjective sensation of nasal airflow and objective measurements (Ecckes, 1998). Reichelmann *et al*., (1999) found unreliability of acoustic rhinometry in pediatric rhinology. Mean cross-sectional areas measured by AR were constantly less than those measured by CT of the nasal cavity up to 33 mm from the nostril, whereas areas measured by AR were greater than

those measured by CT scans beyond that point (Min *et al*., 1995, Mamikoglu *et al*, 2000). AR is not a reliable method for the indication or evaluation of surgery for nasal obstruction (Reber *et al*., 1998).

2.4 Numerical study of flow through the nasal cavity

Better understanding of airflow characteristic in nasal cavity is essential to study the physiological and pathological aspect of nasal breathing. The success of nasal function is highly dependent on the fluid dynamics characteristic of airflow. The anatomical complexity of the nasal cavity makes direct measurements within the nasal cavity highly impossible. CFD has the ability to provide quantitative airflow information at any location within the nasal airway model. These airway models were reconstructed from magnetic resonance (MRI) or computed tomography (CT) imaging data of patients. Recent developments in medical imaging coupled with computational science have opened new possibilities for physically realistic numerical simulations of nasal airflow.

A number of researchers have shown the validity and potential use of CFD in evaluating the flow conditions inside the nasal cavity. Early work regarding this topic was performed by Elad *et al*., (1993) who conducted numerical simulations of steady laminar flow through a simplified nose-like model which resemble the complex anatomy of human nasal cavity using the finite element software package FIDAP (Fluid Dynamics International) (see Figure 2.4). The number of mesh created for this nasal model is approximately <3000 elements. They found that during expiration, flow pattern spread uniformly into nasal cavity until it reached turbinate. The turbinate is an obstacle in the airway that increases the resistance to airflow. The lowest resistance in the model

was located along the floor of the nasal cavity. The flow pattern was also found to be similar during inspiration and expiration but in opposite direction.

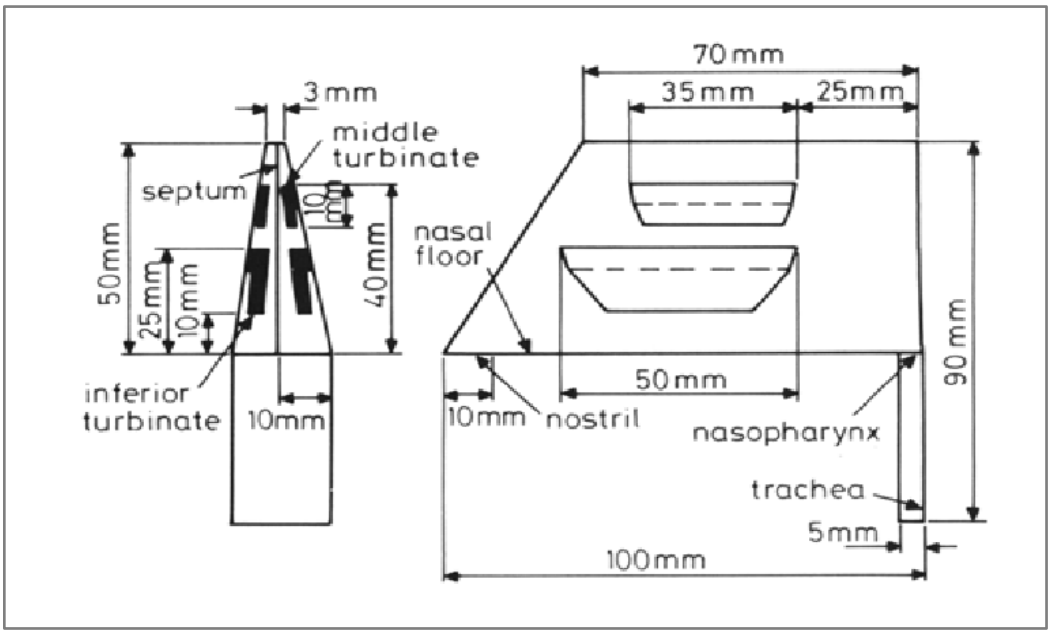

Figure 2.4: Nose-like model- reproduced from Elad et al., (1993)

Due to computational limitation, Naftali *et al*., (1998) in their early work constructed a 2D nose-like model based on averaged data of human nasal cavities to study the transport phenomena of normal and diseased human noses for inspiration under various ambient conditions. They treated the nasal airflow as laminar and simulated the nasal airflow for average breathing rates about 15 m/s with Reynolds number approximately 500. The results demonstrated that the turbinates increase the rate of local heat and moisture transport by narrowing the passageways for air and by induction of laminar swirls downstream of the turbinate wall.

Another early study was that of Keyhani *et al*., (1995) who performed a finite element analysis of steady laminar flow through one side of the human nasal cavity. The

3D nasal model was reconstructed from 42 coronal CAT scans using an imaging software called VIDA (Cardiothoratic Imagaing Research Section, University of Pennsylvania). A computer program was developed in order to convert the coordinate data into a format that could be processed by the mesh generator module of FIDAP. As seen in Figure 2.5, the final domain contained 76,950 brick shape mesh elements.

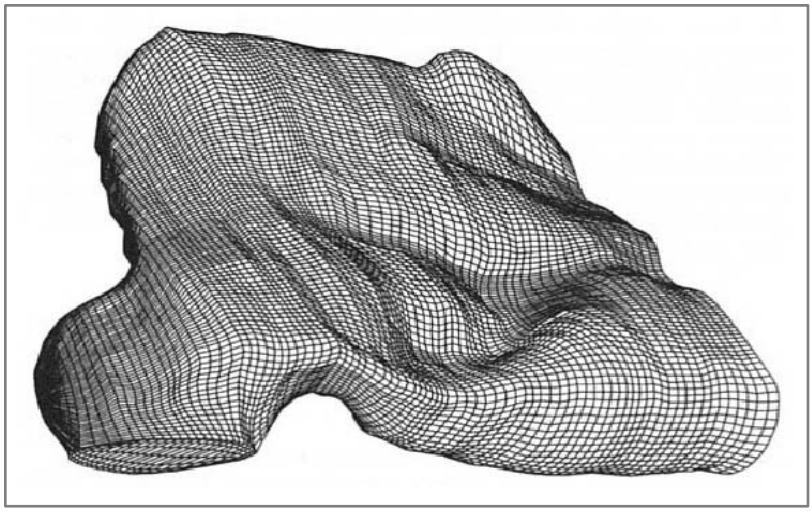

Figure 2.5: Medial slide of the three-dimensional finite element mesh of the right nasal cavity- reproduced from Keyhani et al., (1995)

The laminar flow was simulated for breathing rates of 125 ml/s and 200 ml/s using computational fluid dynamics (CFD) software, FIDAP. Their numerical results were validated with the experimental measurements obtained by Hahn *et al.*, (1993). According to this study, the majority of the airflow passes through the inferior turbinate. Results obtained also confirmed that airflow through the nasal cavity is laminar during quiet breathing.

Airflow in the main nasal cavity is generally described as laminar by several researchers for flow rates of 7.5 L/min to 15 L/min. Segal *et al*., (2008) performed numerical simulation of steady state inspiratory laminar airflow for flow rate of 15 L/min. In their study, three dimensional computational models of four different human nasal cavities which constructed from coronal MRI scans were used (see Figure 2.6). The nasal model then was meshed with hexahedral elements using a semi-automated process MAesh which was developed in-house using Matlab (The MathWorks, Inc., Natick, MA, USA). In their study, they found that in all four nasal models, the majority of flow passed through the middle and ventral regions of the nasal passages. The amount and the location of swirling flow differed among the subjects.

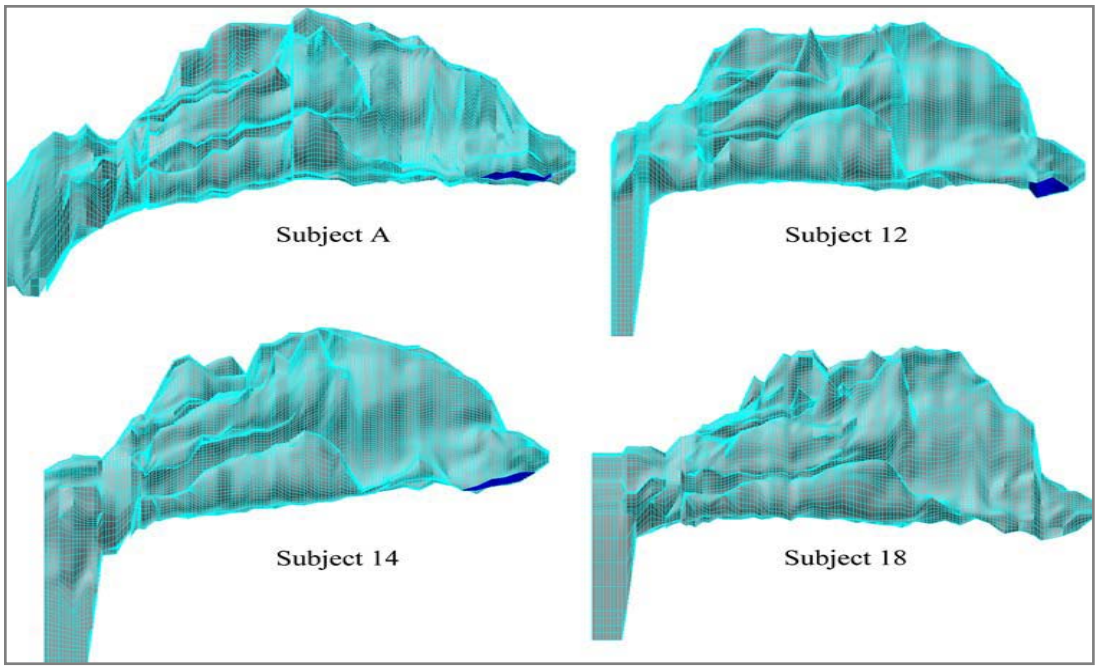

Figure 2.6: Computational meshes for subjects A, 12, 14 and 18. Nostrils are shown in blue on the right side of the models and the nasopharynx is on the left- reproduced from Segal et al., (2008)

Wen *et al*., (2008) also simulated steady laminar nasal airflow for flow rates of 7.5 to 15L/min using computational fluid dynamics software FLUENT. An anatomically correct three dimensional human nasal cavity computed from CT scan images were used (see Figure 2.7). The solution was found to be mesh-independent at approximately 950,000 cells. Results shows that the nasal resistance value within the first 2-3 cm contribute up to 50% of the total airway resistance. Vortices were observed in the upper olfactory region and just after the nasal valve region.

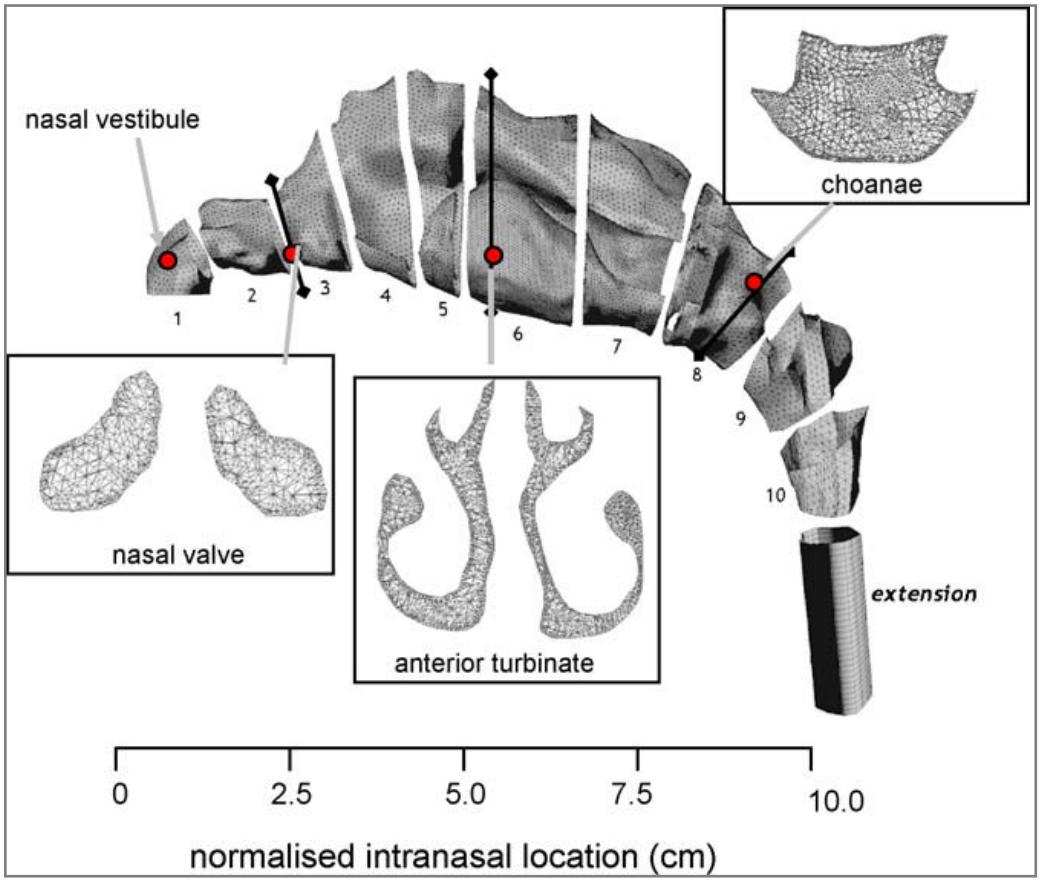

Figure 2.7: Nasal cavity model constructed by Wen et al., (2008)

Inthavong *et al*., (2007) constructed 3D nasal passage based on nasal geometry which obtained through a CT scan of a healthy human nose. A constant laminar flow

rates about 7.5 L/min was used to simulate light breathing. The mesh in the computational domain is unstructured tetrahedral and the size of the mesh is approximately 950,000 cells. The airflow analysis showed vortices present in nasal valve region which enhanced fibre deposition by trapping and recirculating the fibre in the regions where the axial velocity is low.

Another work was done by Croce *et al*., (2006), who also simulated steady state inspiratory laminar airflow for flow rate of 353 ml/s in both nostril using FLUENT. The 3D computational geometry used in Croce *et al*., (2006) numerical study was derived from CT scan images of a plastinated head using a commercial software package, AMIRA (Mercury Computer System, Berlin). The final adapted mesh consisted of 1,353,795 tetrahedral cells. The results obtained from this study shows that airflow was predominant in the inferior median part of nasal cavities. Vortices were observed downstream from the nasal valve and toward the olfactory region.

Other studies include Zamankhan *et al*., (2006), who study the flow and transport and deposition of nano-size particle in a three dimensional model of human nasal passage. The nasal cavity model was contructed from a series of coronal MRI scans. They simulated the steady state flows for breathing rate of 14 L/min and the Reynolds number bases on the hydraulic diameter was about 490. The airflow simulation results were compared with the available experimental data for the nasal passage. They found that, despite the anatomical differences of the human subjects used in the experiments and computer model, the simulation results were in qualitatively agreed with the experimental data.

Several researchers treated the nasal airflow as turbulent flow. Liu *et al*., (2007) constructed 3D human nose model based on coronal CT scans. A nostril pointing downwards was added to the nasal geometry model. Unstructured mesh were created with the size of the mesh was approximately 4,000,000 elements. Turbulent flows were simulated for inhalation flow rates ranging from 7.5 to 60 L/min by using Reynolds Averaged Navier-Stokes (RANS)/ Eddy Interaction Model (EIM). Large Eddy Simulation (LES) modelling was simulated for intermediates flow rates of 30 and 45 L/min. The simulations study showed that the total particle deposition result using LES indicate that the particle deposition efficiency in the nasal cavity show better agreement than standard RANS/EIM approach when compared to the in vivo data.

Zhao *et al*., (2006) also treated the nasal airflow as turbulent in their study. They constructed 3D nasal model based on CT scans in order to investigate the left nasal valve airway which was partially obstructed. Then, they modified the nasal valve region volume to simulate the narrowing of the nasal valve during human sniffing. The airflow was assumed as turbulent and total nasal flow rates was between 300 and 1000ml/s. Result from this study revealed that the increase in airflow rate during sniffing can increase odorant uptake flux to the olfactory mucosa but lower the cumulative total uptake in the olfactory region when the inspired air/odorant volume was held fixed.

Another nasal airflow analysis using the turbulence model was conducted by Mylavarapu *et al*., (2009). They investigated the fluid flow through human nasal airway model which was constructed from axial CT scans. TGRID was then used to create an unstructured hybrid volume mesh with approximately 550,000 cells. Flow simulations and experiments were performed for flow rate of 200 L/min during expiration. Several different numerical approaches within the FLUENT commercial software framework

were used in the simulations; unsteady Large Eddy Simulation (LES), steady Reynolds-Averaged Navier-Stokes (RANS) with two-equation turbulence models (i.e. k-epsilon, standard k-omega, and k-omega Shear Stress Transport (SST)) and with one-equation Spalart-Allmaras model. Among all the approaches, standard k-omega turbulence model resulted in the best agreement with the static pressure measurements, with an average error of approximately 20% over all ports. The largest pressure drop was observed at the tip of the soft palate. This location has the smallest cross section of the airway.

Numerical study on human nasal airflow with abnormal nasal cavity cause by several chronic diseases also has been the subject of several studies. Wexler *et al*., (2005) constructed 3D nasal model of a patient with sinonasal disease. They investigated the aerodynamic consequences of conservative unilateral inferior turbinate reduction using computational fluid dynamics (CFD) methods to accomplish detailed nasal airflow simulations. Steady-state, inspiratory laminar airflow simulations were conducted at 15L/min. They found that inferior turbinate reduce the pressure along the nasal airway. Also, the airflow was minimally affected in the nasal valve region, increased in the lower portion of the middle and posterior nose, and decreased dorsally.

Garcia *et al*., (2007) constructed 3D nasal geometry by using medical imaging software (MIMICs, Materialise) to investigate airflow, water transport, and heat transfer in the nose of an Atrophic Rhinitis (AR). The patient underwent a nasal cavity-narrowing procedure. Rib cartilage was implanted under the mucosa along the floor of the nose, and septum spur was removed. The reconstructed nose was simulated and the nasal airflow was assumed as laminar with 15 L/min corresponding to resting breathing rate. This study showed that the atrophic nose geometry had a much lower surface area

than the healthy nasal passages. The simulations indicated that the atrophic nose did not condition inspired air as effectively as the healthy geometries.

Lindemann *et al*., (2005) produced 3D model of human nose to investigate the intranasal airflow after radical sinus surgery. The human nasal model was constructed based on CT scans of the nasal cavities and the paranasal sinuses of an adult. The numerical simulation was performed by assuming the nasal airflow as laminar at 14 L/min for quiet breathing rate. Result showed that aggressive sinus surgery with resection of the lateral nasal wall complex and the turbinates cause disturbance of the physiological airflow, an enlargement of the nasal cavity volume, as well as an increase in the ratio between nasal cavity volume and surface area.

2.5 Gender comparison

Several researchers have shown the benefits of computational fluid dynamics (CFD) in better understanding of flow through the nasal cavity. Some of the main players are Wen *et al*., (2008), Mylavarapu *et al*., (2009), Segal *et al*., (2008), Weinhold *et al*., (2004), Xiong *et al*., (2008). However, most of the researchers employed male human subject in the determination of the nasal patency. Inter human anatomical differences exists and also differences on anatomical and physiological morphology are observed based on gender. No specific numerical modelling studies have been carried out to compare and ascertain the effect of gender on flow variable inside the nasal cavity. Gender differences is said to be the important determinant of clinical manifestations of airway disease. Even though obstructive sleep apnea, is prevalent in both the gender, its effect on male subjects is more prominently observed (Rowley *et al*.,

2002). Also a higher prevalence of irregular breathing phenomenon among men when compared to women during sleeping and also the fact that men have a larger upper airways in sitting and supine positions (Thurnheer *et al*., 2001) makes it all the more important to study the effect of gender on breathing phenomenon. It would be an importance too to study the effect of anatomical variation based on gender on the flow parameter.

2.6 Gravity Effect

Also CFD modelling involves various simplifications, for example the postural effects which drastically affect the outcome of the analysis. The postural changes in nasal airway resistances are of clinical importance when accessing patients with nasal obstruction. Mohsenin, (2003) demonstrated the effect of decrease in pharyngeal cross sectional area and occurrence of OSA. The gravitational force is considered to be one significant determinant of the closing pressure (Watanabe *et al*., 2002). Study performed by Tvinnereim *et al*., (1996) showed that nasal and pharyngeal resistance doubles upon assumption of supine posture; however the difference obtained was not statistically significant. Beaumont *et al*., (1998) found that at sea level, gravity forces that cause the soft palate and tongue to fall back in the supine posture would narrow upper airways in all its length. A study by Hsing-won Wang, (2002) on the effect of posture on nasal resistance varied from 0.612 Pa/mL/sec in sitting position to 0.663Pa/mL/sec in the supine position.

Matsuzawa *et al*., (1995) observed that the MRI data obtained in supine, lateral and prone position revealed that the upper airway was narrowest in the supine position, and widest in the prone position indicating the anatomical narrowing of the upper airway especially the pharyngeal area. Martin *et al*., (1995) showed in the supine position all the upper airway dimensions decreases with increasing age in both men and women, except the oropharyngeal junction. Hence, it is very important to study the effect of gravity on the flow through the nasal cavity.

2.7 Plug flow and pull flow boundary condition

Keyhani *et al*., (1995), Wexler *et al*., (2005), Zamankhan *et al*., (2006), Segal *et al*., (2008), and Ishikawa *et al*., (2009) constructed 3D nasal computational models and simulated the airflow by utilizing plug flow boundary condition. For plug flow, fixed airflow rate with a uniform velocity profile was imposed at the nostril. While a stress free boundary condition was used at the outflow boundary condition. On the other hand, the pull flow boundary condition is based on negative pressure set at the nasopharynx. Garcia *et al*., (2007) used pull flow boundary condition to study the airflow and water transport simulation in the nasal cavity. Wexler *et al*., (2005) also attempted to conduct the nasal airflow simulation using pull flow boundary condition. However, this simulation has been unsuccessful due to the failure of residuals to converge. There is still no unanimity among the researchers with respect to the use of exact boundary conditions. Most researchers employed the plug flow model in order to stimulate the flow features inside the nasal cavity. The natural physiological inspiratory mechanism is based on pull flow conditions, wherein the expansion of the lungs sets in negative

pressure gradient enabling the air from the ambient atmosphere to rush inside the nasal cavity through the nostril inlets.

2.8 Summary

In summary, the literature reviewed shows that all the previous numerical studies on nasal airflow have generalized the behavior to both gender. No specific numerical modelling studies have been carried out to compare and ascertain the effect of gender on flow variable inside the nasal cavity. Also CFD modelling involves various simplifications, for example the postural effects which drastically affect the outcome of the analysis. It was also found that there is no unanimity with respect to the use of exact boundary conditions. Hence there is no standardization of the boundary definition with respect to the study concerning the nasal flow using numerical methods. Therefore the current work will investigate the effect of different boundary condition on nasal airflow behavior through the human nasal cavity. Also the effects of gravity and posture on flow properties inside the nasal cavity will be investigated. Finally, the gender effect on nasal airflow characteristic due to variation in nasal anatomy will be studied.

CHAPTER 3

METHODOLOGY

3.1 Overview

This chapter presents the method used to reconstruct the three-dimensional model of the human nasal cavity, mesh generation and numerical setup for the nasal airflow simulation. The overall process of the present numerical study has been illustrated in the flow chart below.

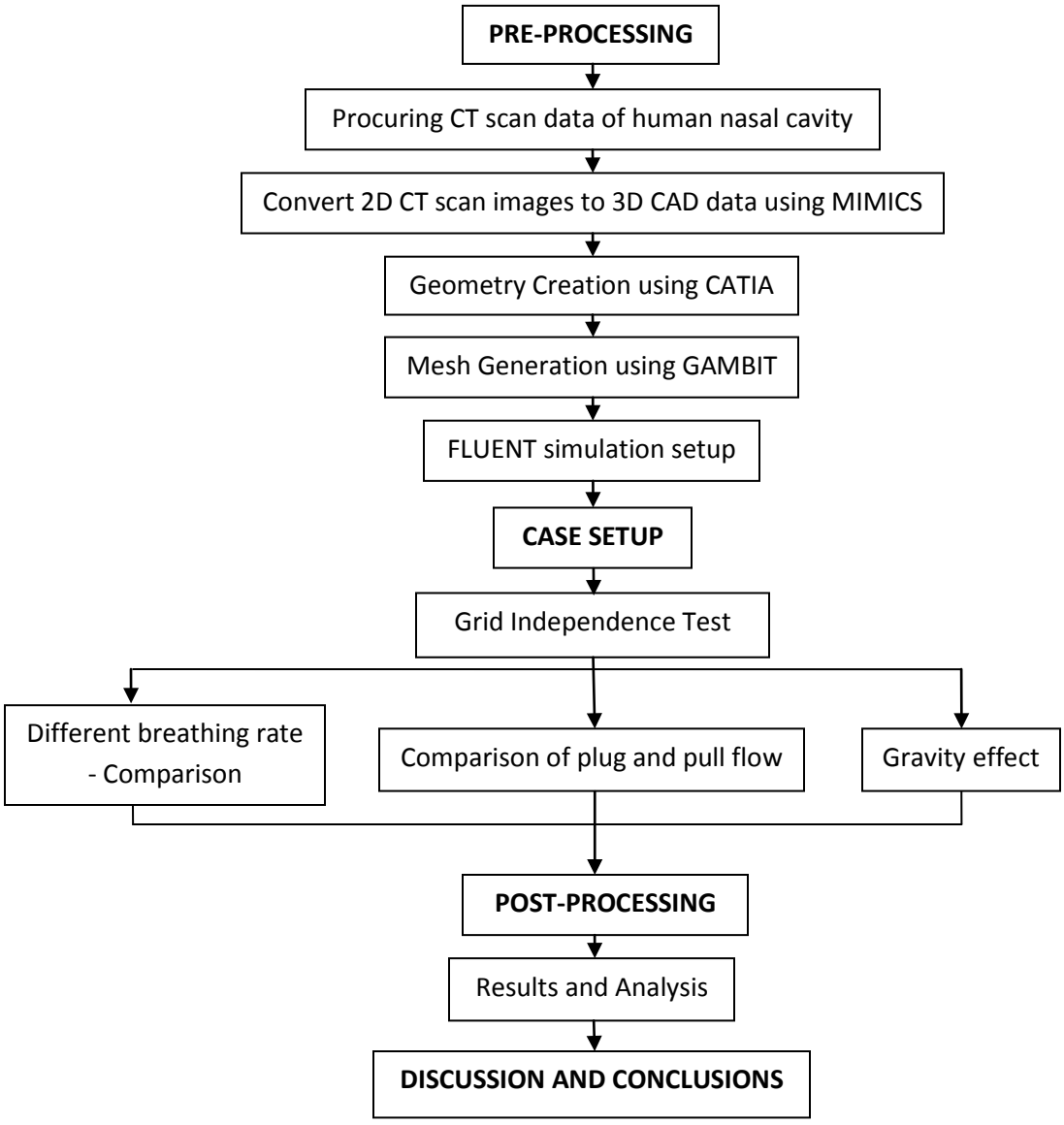

3.2 3D computational model of the nasal cavity

Reconstruction of 3D anatomical model of the human nasal cavity can be very time consuming. The general process of developing the 3D anatomical model basically consist of selection of CT scan data of human nasal cavity followed by converting the 2D CT scan images into 3D CAD data using medical image processing software, MIMICs and finally construct the surface geometry by using CAD software, CATIA.

3.2.1 Procuring CT scan data of human nasal cavity

The anatomical model of the nasal airway used for this numerical study was derived from CT scan images of a healthy 39 year old Malaysian female. The CT scan image of the nasal airway was taken from pre-existing CT scan data sourced from Universiti Sains Malaysia, Medical Campus Hospital. The nasal anatomy was attested to be normal by the ear, nose and throat (ENT) surgeon. Figure 3.1 shows a series of coronal CT scan images along the axial distance of the nasal cavity of the female human subject. The scans produced a total 385 slices of axial, coronal and sagittal images which accounted for the complete nasal cavity area, from nostril to nasopharynx.

The increment between each slice of the scan images is 0.8mm and the scan pixel resolution is 0.434mm. It is important to make sure that the scan interval is less than 2 mm in order to accurately capture the complex geometry of the nasal cavity and to avoid stair-step artifact which usually appear on the curved surface of the model (Bailie *et al*., 2006). However, reduction of the layer thickness requires more expensive machines and a slower build process. The CT scan data was imported into medical image processing

software MIMICs for the reconstruction of the 3D human nasal cavity for this case study.

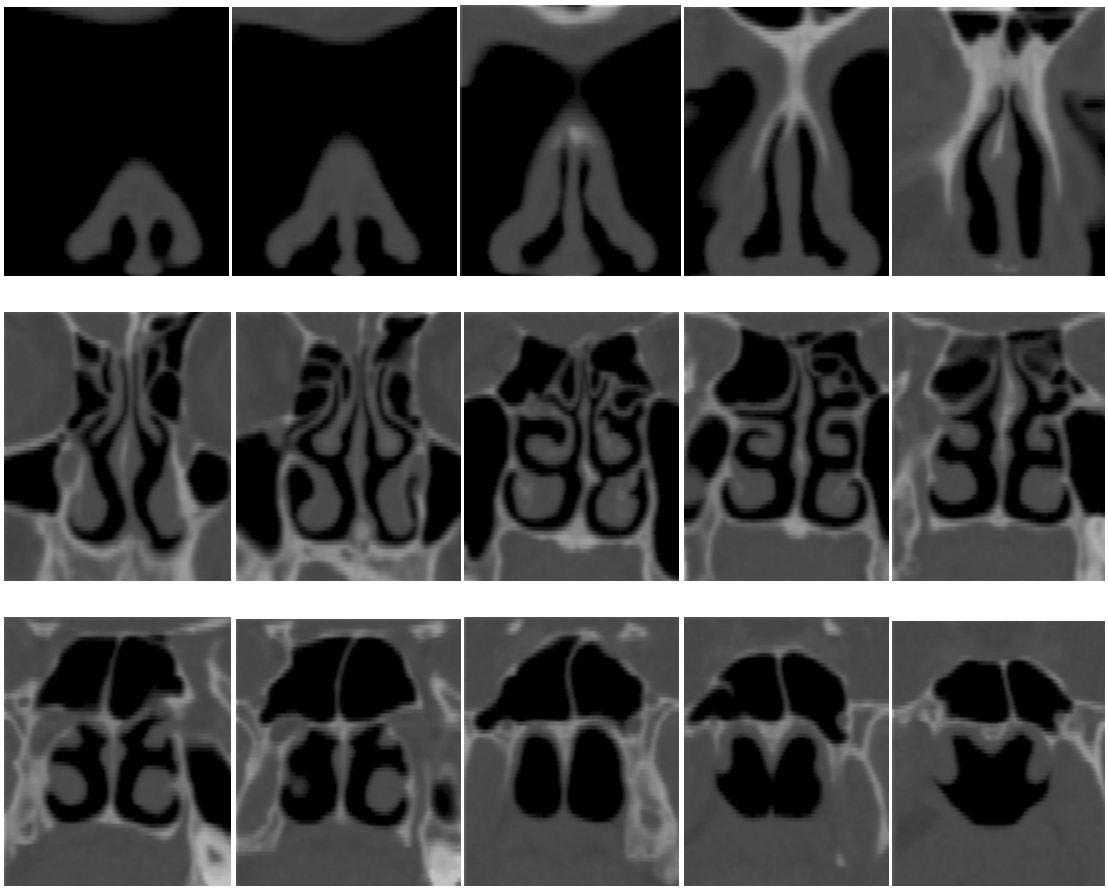

Figure 3.1: Coronal CT scan images along the axial distance of the human nasal cavity

3.2.2 Convert 2D CT scan images to 3D CAD data using MIMICs

MIMICs is an image processing and editing software which provides the tool for the visualization and segmentation of CT images and also for the 3D rendering of objects. Before the scan data can be processed, MIMICs reads the 2D CT scan images from the DICOM (*.dcm) file format and convert it into MIMICs (*.mcs) file format.

MIMICS will compress and merge all the axial, coronal and sagittal scan images into a single volume file project based on the similar pixel size value.

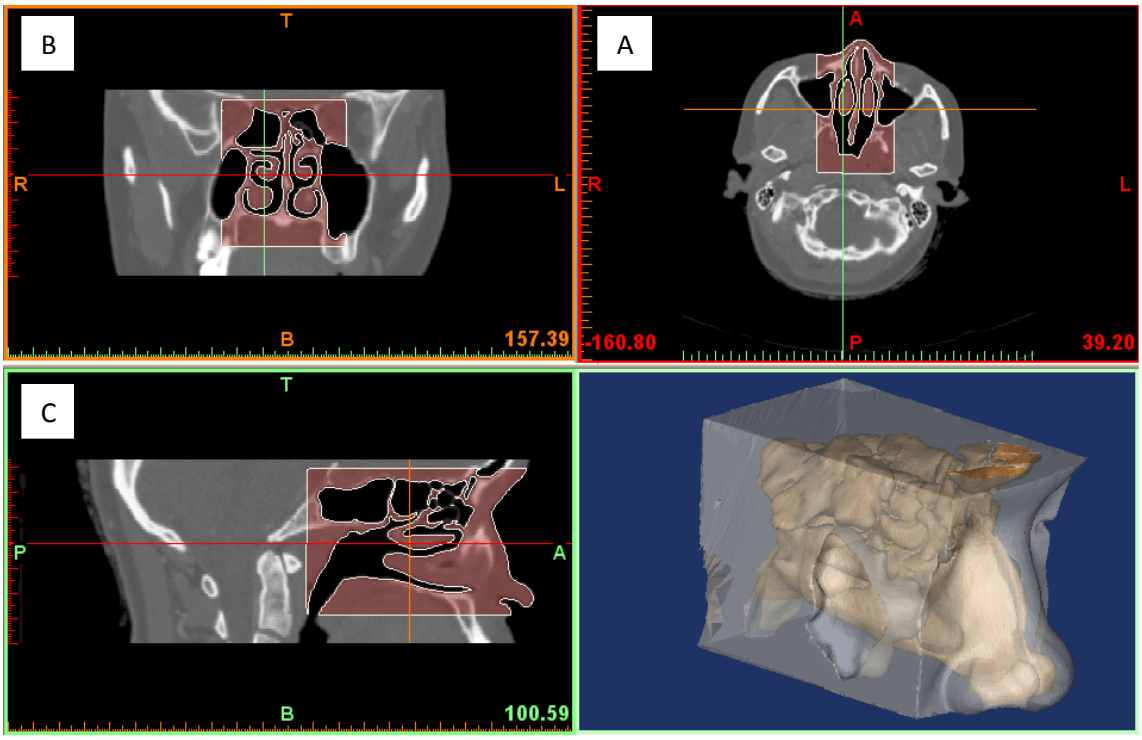

Figure 3.2: CT scan images from A: axial, B: coronal and C: sagittal plane and 3D model of the female human nasal cavity

The main step of nasal geometry reconstruction from the CT scan data is the segmentation process in which the regions of interest, nasal passage is identified. The segmentation was developed based on the Hounsfield Units (HU) in the CT images. HU is a measure of the electron density of the tissue. Segmentation was performed by defining a range of threshold values to create the segmentation mask. The range of the threshold value used for this case study is between -444 to 2037 HU (see Figure 3.2). A correct threshold value is vital in capturing the important features of the nasal cavity. The threshold value is used to differentiate between bone and soft tissues and to

determine the set of structures to be included in the 3D nasal model. Medical reconstruction requires a good understanding of anatomy, which can only come with experience, and understanding the types of tissue that are preferentially imaged by radiographers. Hence the presence of an expert radiologist and ENT practitioner is essential in deciding the threshold and editing of the geometry.

An automatic region growing function was used to reconstruct the nasal airway from the nostril to nasopharynx based on the segmented mask. The purpose of the region growing function was to reduce the noise, remove floating pixels and to split the unconnected structure. However, manual segmentation is also required to edit the mask which leak to surrounding region and remove the unwanted parts which are still connected to the nasal cavity model. Manual editing function also makes it possible to draw and restore parts of image on the segmented mask. By using the MIMICs editing tools, the scan images were segmented slice by slice on axial, coronal and sagittal plane by using the local threshold value.

MIMICs has the ability to generate and display the 3D anatomical model of the nasal cavity from the segmented scan images. After all the necessary threshold editing, the 3D anatomical model of the nasal cavity was generated from the segmented mask. By using the 3D rendering tools, the 3D nasal cavity model was examined to ensure the suitability of the selected threshold and to confirm the presence of all the required structure for the physical anatomical model.

MIMICs also provide the export function which can be use to export the 3D object produced from the segmented CT scan images into IGES file and can be directly used in any CAD system. As seen in Figure 3.3, the polylines was created based on the segmented mask of the 3D object on each slice of the project by using ‘calculate polyline

function'. Later the 3D polylines data was exported as IGES (*.igs) file format, for the surface model generation using the CAD software, CATIA.

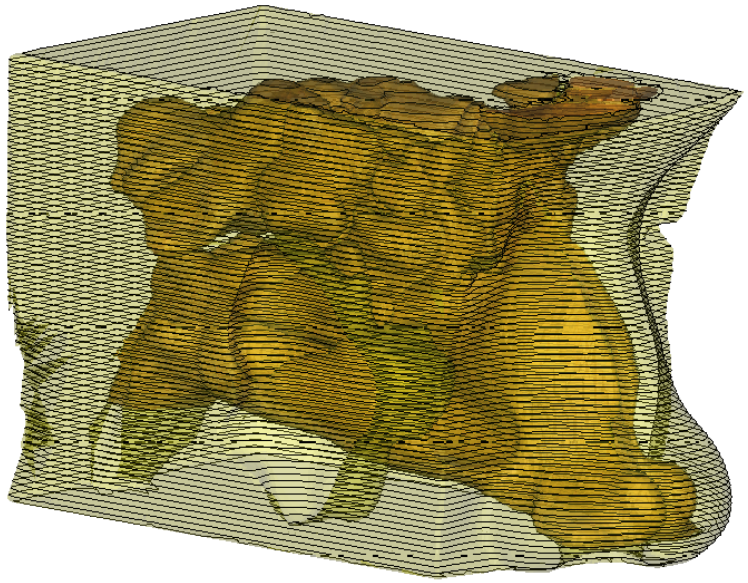

Figure 3.3: Polyline data of the 3D human nasal cavity

3.2.3 Geometry creation using CATIA

The coordinates of the contour point extracted from the CT scan data of the human nasal cavity was imported into CAD software package, CATIA using Digitized Shape Editor (DSE) workbench for surface model generation. DSE is usually used at the initial stages of the reverse engineering and it also provides tools for various operations on the imported digitized data. The IGES (*.igs) file can be imported and displayed in DSE workbench in the form of cloud of points or polylines. However, due to anatomical

complexity, it is not possible to edit and manipulate the 3D anatomical model in the cloud of points form.

Therefore, facets were created directly from the polylines which is as shown is Figure 3.4a using the mesh creation tools. The neighborhood parameter value was set to 7.5mm to define the maximum length of the facet edge. The function of the neighborhood value is to close the unwanted holes of the mesh. Increasing the neighborhood parameter will lead to a non manifold mesh. After the mesh surfaces have been created from the polylines, the next stage is to edit the 3D nasal mesh geometry by removing the unwanted mesh part. As seen in Figure 3.4d, all the paranasal sinuses have been removed in order to simplify the geometry and to reduce the computational cost. Editing was carefully carried out to preserve the original shape of the anatomical model of the human nasal cavity (see Figure 3.4e).

By using the cleaning mesh function, the defective mesh was removed to improve the quality of the mesh. The mesh cleaner helped analyze and delete all the defective mess which consisted of non manifold edges, non manifold vertices, isolated triangle, triangle with inconsistent orientations and the corrupted triangles. After all the necessary mesh cleaning, the 3D mesh geometry was smoothened using the mesh smoothing tool to improve mesh surface quality. Finally, the 3D computational model of the human nasal cavity was created based on the smooth mesh surface by using the automatic surface tool in Quick Surface Reconstruction workbench. Figure 3.4f shows the final 3D model of the nasal cavity obtained from CATIA which can be used for computational modelling.

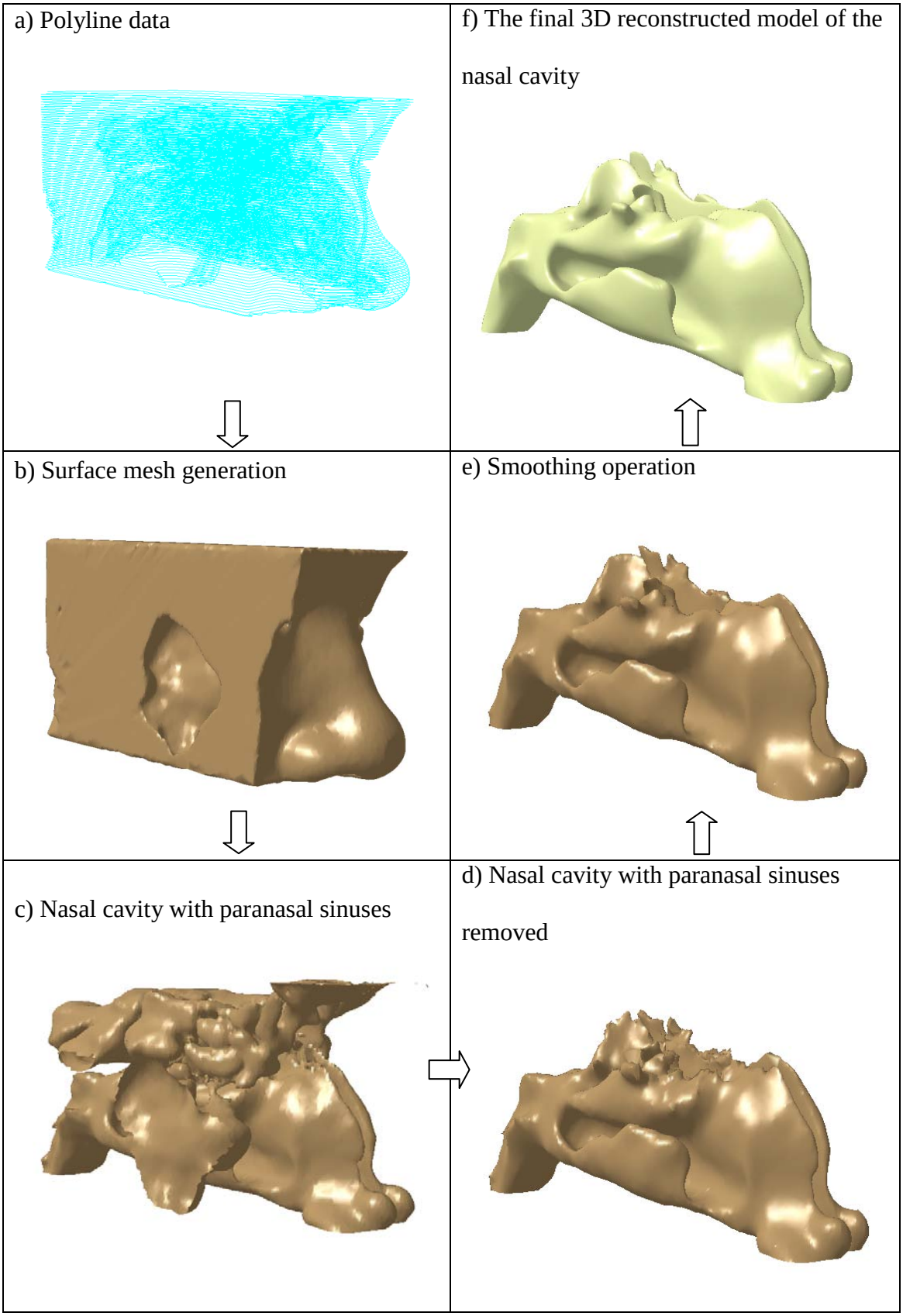

Figure 3.4: Steps involved in developing 3D model of the nasal cavity using CATIA

3.3 Mesh generation using GAMBIT

The 3D anatomical model of the human nasal cavity was imported into GAMBIT using STEP (*.stp) file format where the surface generated are detected as faces. Figure 3.5 shows the multiple faces of the nasal geometry. The multiple faces are then stitched together to form a complete volume which acts as the airflow domain. Before performing the face mesh generation, the nasal geometry was simplified by merging all the small faces into one face. This step is important in order to control the quality of the face and volume mesh of the domain to avoid creating high aspect ratio and highly skewed mesh.

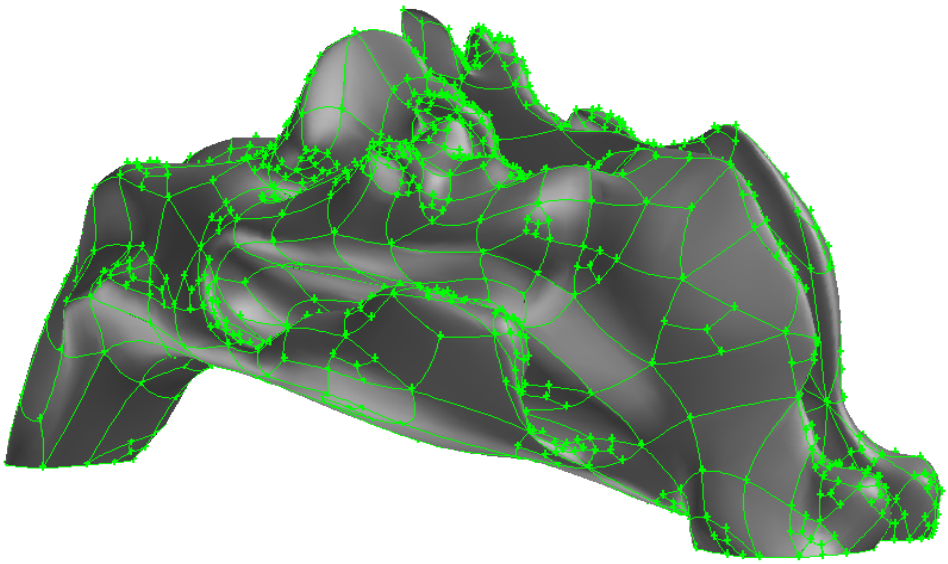

Figure 3.5: 3D computational model of the nasal cavity with surface geometry

A mesh with highly skewed cells can decrease accuracy and destabilize the solution. CFD simulations with structured grids usually give faster solutions compared

to unstructured grids. However, in the present case, due to the anatomical complex structure of the human nasal cavity, it is not only time consuming but almost impossible to create structured grids. Hence, unstructured mesh consisting of tetrahedral elements is preferred for developing the mesh.

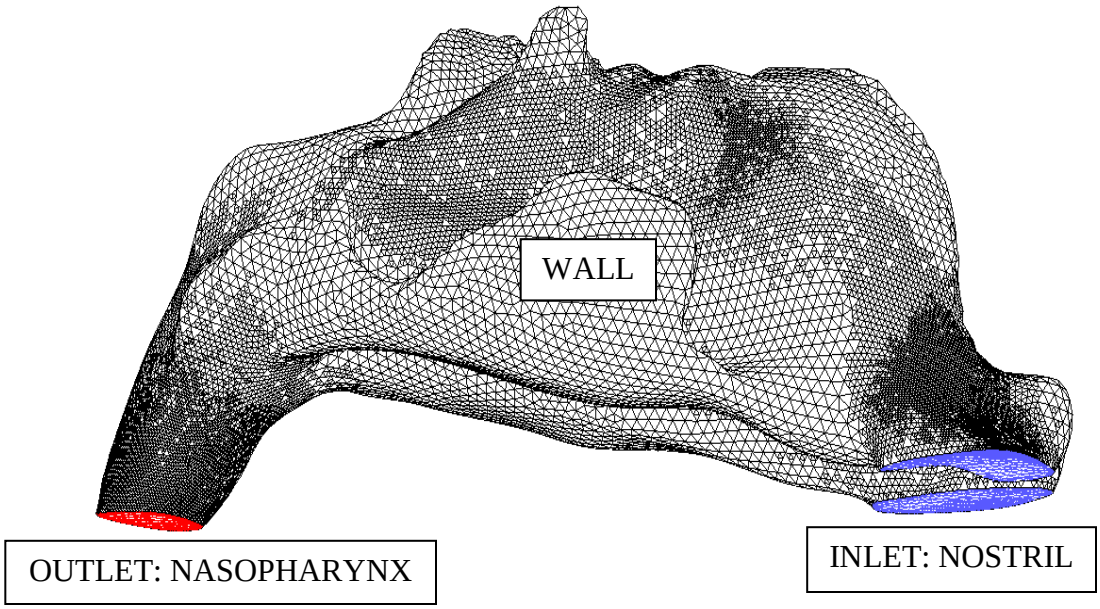

Figure 3.6: Volume mesh of the 3D computational model of human nasal cavity

The accuracy of the CFD study depends primarily on quality and quantity of the mesh distribution. An initial model with 106,393 cells was created and used to solve the airflow field at a flow rate of 7.5L/min. The schematic diagram of the grid is show in the Figure 3.6. The grid independency test was carried out using the gradient adaptation technique. The original mesh was refined based on the velocity gradient. This process was repeated, with each repetition produce a model with a higher cell count than the previous model.

The grid independence test resulted in an optimized grid with 577,010 elements. This was considered sufficient taking into account the computational time and system

memory. Variation in pressure and velocity with higher grid were negligible. Hence, the mesh with 577,010 elements was used for our simulation. In order to ensure the accuracy of the flow simulation near the wall surfaces, the y+ values obtained for the nasal cavity model is less than 5. The wall y+ value is the distance between the cell centroid to the wall for wall-adjacent cell.

$$y^+ = \frac{u_\tau y}{v} \tag{3.1}$$

Where y is the normal distance of the first grid point from the wall, u_τ is the friction velocity and v is the kinematic velocity of the fluid flow.

3.4 Numerical analysis

This sub-chapter provides the governing equations for the current fluid flow problem and numerical models used for the numerical simulation.

3.4.1 Governing equation

CFD is fundamentally based on the governing equations of fluid dynamics. They represent mathematical statements of the conservation laws of physics. For a general fluid property defined by Φ, can be cast into transport equation form as:

$$\frac{\partial(\rho\Phi)}{\partial t} + div(\rho\Phi\boldsymbol{u}) = div(\Gamma grad\Phi) + S_\Phi \tag{3.2}$$

The first and second terms on the left are time derivative term and the convective terms. The terms on the right are the diffusive terms and the source terms. In words, equation above can be read as:

Rate of increase of Φ in a fluid element	+	Net rate of flow of Φ through a fluid element	=	Rate of increase of Φ due to diffusion	+	Rate of increase of Φ due to additional sources	

The governing equation of fluid flow for an incompressible fluid, such as the airflow in the respiratory system can be written as:

$$\frac{\partial \Phi}{\partial t} + \frac{\partial (u\Phi)}{\partial x} + \frac{\partial (v\Phi)}{\partial y} + \frac{\partial (w\Phi)}{\partial z} = \frac{\partial}{\partial x}\left[\Gamma \frac{\partial \Phi}{\partial x}\right] + \frac{\partial}{\partial y}\left[\Gamma \frac{\partial \Phi}{\partial y}\right] + \frac{\partial}{\partial z}\left[\Gamma \frac{\partial \Phi}{\partial z}\right] + S_{\Phi} \qquad (3.3)$$

Where t is time, u, v, w represent velocity components, Γ is the diffusion coefficient, and S_{Φ} is a general source term. This equation is commonly used as the starting point for computational procedures in the finite volume method.

3.4.2 Turbulence models

In the current study, the simulation is based on the numerical solution of the Reynolds Averaged Navier-Stokes equation representing the general equation for 3D flow of incompressible and viscous fluids. The SST k-ω turbulence model, a two equation turbulence model was employed. The SST k- ω model accounts for transport of

turbulent shear stress and gives highly accurate predictions of the amount of flow separation under adverse pressure gradient.

The SST model is a blend between the k-ω turbulence model, which is applicable near the walls, and the k-ε turbulence model which is applied at the core of the computational domain, with an additional limiter in the formulation of the eddy viscosity to provide proper account of the turbulent SST. Therefore SST combines the advantages of both the k-ε and k-ω methods. The k-ω turbulence model has a near wall treatment allowing accumulation of nodes towards the wall without any special non-linear damping function, whereas the k-ε model is less sensitive to free stream and inlet conditions.

The combination is ideal for a flow in a complex geometry like the nasal cavity (Liu *et al.*, 2007). The suitability of SST k-ω model also has been experimentally validated by Mylavarapu *et al.*, (2009), Ahmad *et al.*, (2010) and Zubair *et al.*, (2010).

3.4.3 Numerical solver procedure

The governing transport equations were discretized using the control volume based technique. The domain is discretized into control volumes based on the created computational mesh. The governing equations were converted into integral form to allow integration of the equation on each computational mesh. A set of algebraic equations for dependent variables such as velocities, pressure and temperature are then set up and solved.

The segregated pressure based solver within FLUENT was chosen which solved the governing equations. Figure 3.7 shows the flow chart of the iteration procedure based on the segregated pressure-based solution method. FLUENT stores discrete values of the scalar Φ at the cell center. However, face values Φf required for convection terms and must be interpolated from the cell center values. This is accomplished by using an upwind scheme.

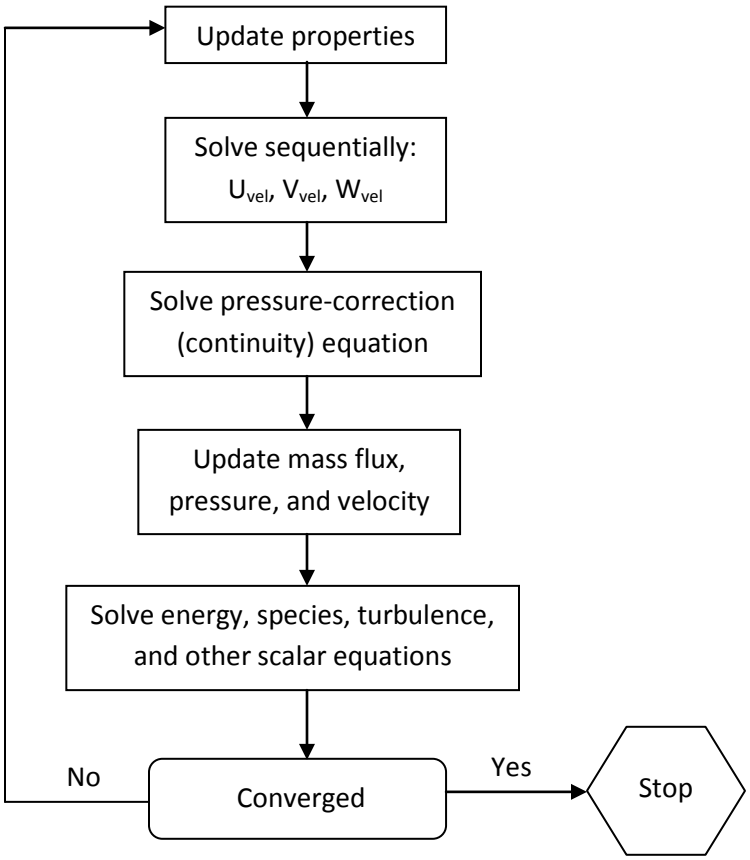

Figure 3.7: Pressure-based solution method (FLUENT User manual)

In the present study, first order upwind scheme was used initially to stabilize the flow. Smaller under relaxation factors value was applied in order to gain flow stability. After the first order converged, the second order upwind scheme was then utilized to

accomplish higher order accuracy of the flow solution. The quality of the second order upwind scheme has been proved for its reliability and accuracy in evaluating the scalar variables on unstructured meshes (FLUENT User manual).

The SIMPLE algorithm was used to obtain the relationship between velocity and pressure corrections to enforce mass conservation and also to obtain the pressure. Convergence was considered complete only when the residuals for all equations dropped by six order of magnitude (10-6) and when the residuals had flat-lined.

3.4.4 Boundary condition definition

The boundary conditions are defined in Table 3.1. The nasal wall was assumed to be rigid and the simulation ignored the presence of mucus. A no-slip boundary condition was defined at the walls. For plug flow inspiration case, mass flow rate was imposed at the nostril inlet and outflow boundary was defined at the nasopharynx outlet. Since, the velocity or pressure at the nasopharynx are not known prior to solution of the flow problem, we used outflow boundary condition to model the nasopharynx exit during inspiration. Expiration for plug flow was defined as pressure outlet at the nostril and mass flow rate at the nasopharynx.

Table 3.1: Boundary condition for pull flow and plug flow

		Inspiration	**Expiration**
PLUG FLOW	Inlet	Mass flow inlet	Pressure outlet
	Outlet	Outflow	Mass flow inlet
PULL FLOW	Inlet	Inlet Pressure	Pressure outlet
	Outlet	Pressure outlet	Pressure inlet

The pull flow inspiration model was simulated using negative pressure value set at the nasopharynx and pressure inlet with athmospheric pressure equivalent of 0 Pa was adopted at nostrils accounting for the desired mass flow rate. An expiration case was simulated using pressure outlet at the nostril and positive pressure value defined at nasopharynx. The pressure gradient was selected so as to maintain the required mass flow rate entering the system.

Steady state laminar and turbulent airflow simulations were modelled. At 15L/min the Reynolds number obtained at the nostril inlet was around 1,600 and for 20L/min the Reynolds number was 3,100. The airflow was therefore laminar for flow rates up to 15L/min and the flow was treated as turbulent flow beyond 15L/min. This was also in general agreement with previous researchers (Wen *et al*., 2008, Segal *et al*., 2008), who determined laminar nature of the flow, for flow less than 15 L/min.

In turbulent flow computations, additional boundary conditions for turbulence parameters need to be specified at inlet locations. Turbulent intensity at the nostril inlet was set to 5%, and the viscosity ratio value is 10 (Liu *et al*., 2007). The simulation was carried out on an IBM platform, Intel, Xenon(R) CPU, 2GB RAM which typically took nearly to 2 days to complete the simulation.

CHAPTER 4

RESULTS AND DISCUSSION

4.1 Overview

This chapter presents and discusses the results obtained from the numerical simulation of the human nasal cavity. Each of the cases studied are presented as different subchapters. The case study includes the basic understanding of the nasal physiology, comparison between different flow rates for both inspiration and expiration, effect of gender based anatomical variations on the nasal airflow, gravity effect and boundary condition prescription for nasal airflow simulation.

4.2 Grid dependency analysis

A grid dependency study has been performed for the nasal cavity computational model. The model was initially developed using unstructured tetrahedral mesh with 106,393 numbers of elements. Gradient adaptation was performed based on the average velocity values obtained from the nasal airflow simulation during inspiration for flow rates of 7.5 L/min. As seen in Figure 4.1, the grid independence test has been conducted in the same nasal cavity model with different size of mesh. Each adaptation resulted in a new mesh and the variation in velocity parameter was noted for different locations till the variations were negligibly small.

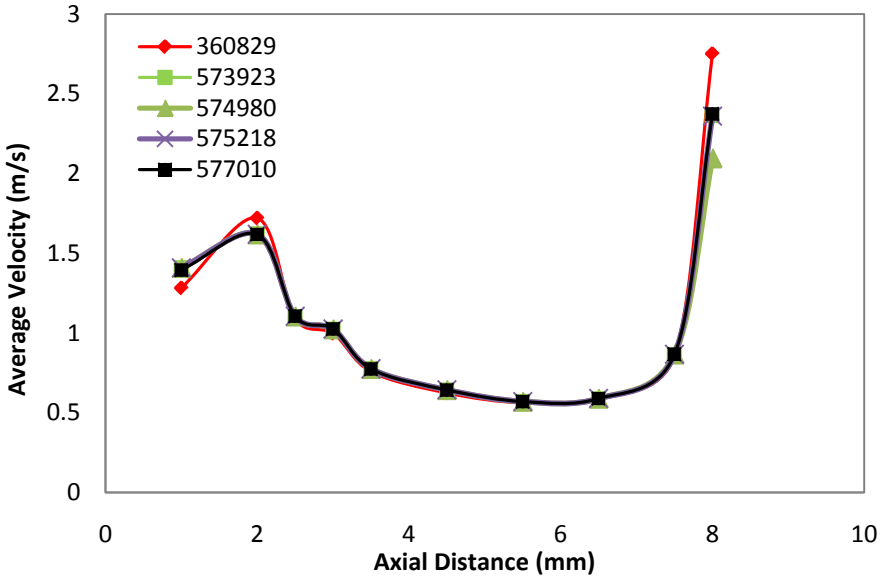

Figure 4.1: Grid independence plot

The results obtained shows that the average velocity values do not change as the mesh resolution increased to 591878. Hence, the mesh with 577010 elements was used for our simulation. This was considered sufficient taking into account the computational time and system memory. Near wall model approach was applied, where the mesh close to the wall was refined in order to resolve the near wall flow for turbulent airflow. In order to ensure the accuracy of the flow simulation near the wall surfaces, the $y+$ values obtained for the nasal cavity model is less than 5.

4.3 Geometry comparison

Figure 4.2 shows the ten planes created along the axial distance of the nasal cavity. Ten cross-sectional areas were created and used to calculate the flow properties as shown in Figure 4.2. The nasal cavity extends from anterior to posterior region along the axial length. The anterior region of the nasal cavity is in the range of $x \leq 3$ cm and the posterior region is in the range of $x > 5$ cm. The planes were created perpendicular to the airflow through the nasal cavity.

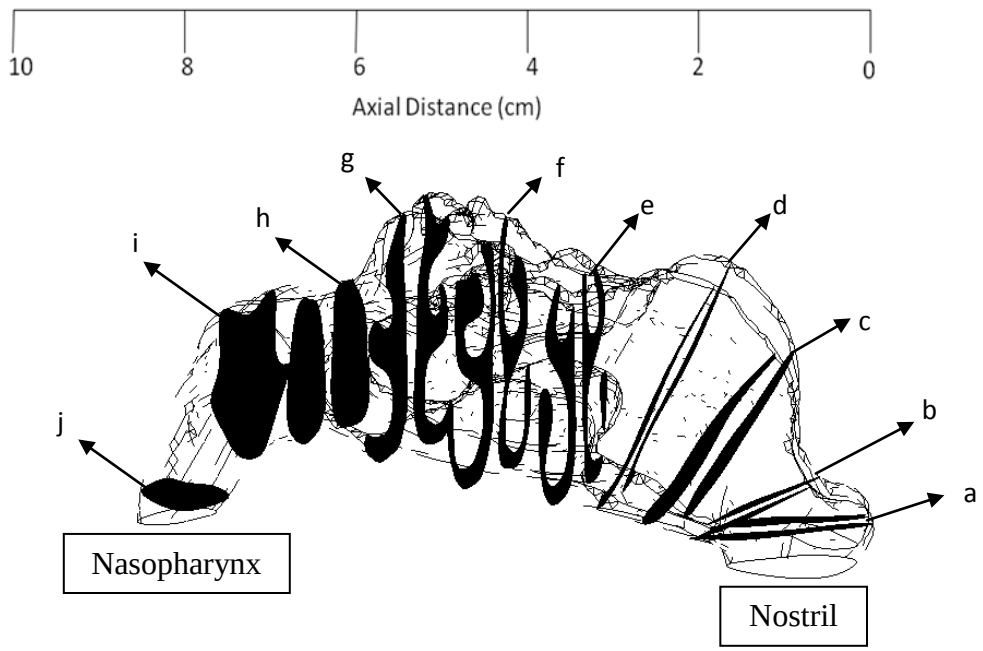

Figure 4.2: Ten cross section area along the axial distance of the nasal cavity

The first plane, Figure 4.3a, which is located at the nostril was created to capture the flow characteristic at the vestibule region. Figure 4.3b shows the smallest cross section area of the nasal cavity which represents the nasal valve region. The planes in Figure 4.3c and 4.3d were produced in order to capture the flow feature at the diverging

region after the nasal valve location and before the airflow enter the turbinate section. Planes in Figure 4.3e, 4.3f and 4.3g allow capturing flow pattern through the inferior, middle and superior turbinate region. It is also important to study the flow characteristic near nasopharynx (Figure 4.3h) and at the nasopharynx region at (Figure 4.3i). Figure 4.3j shows the plane created to capture the airflow through the nasal outlet.

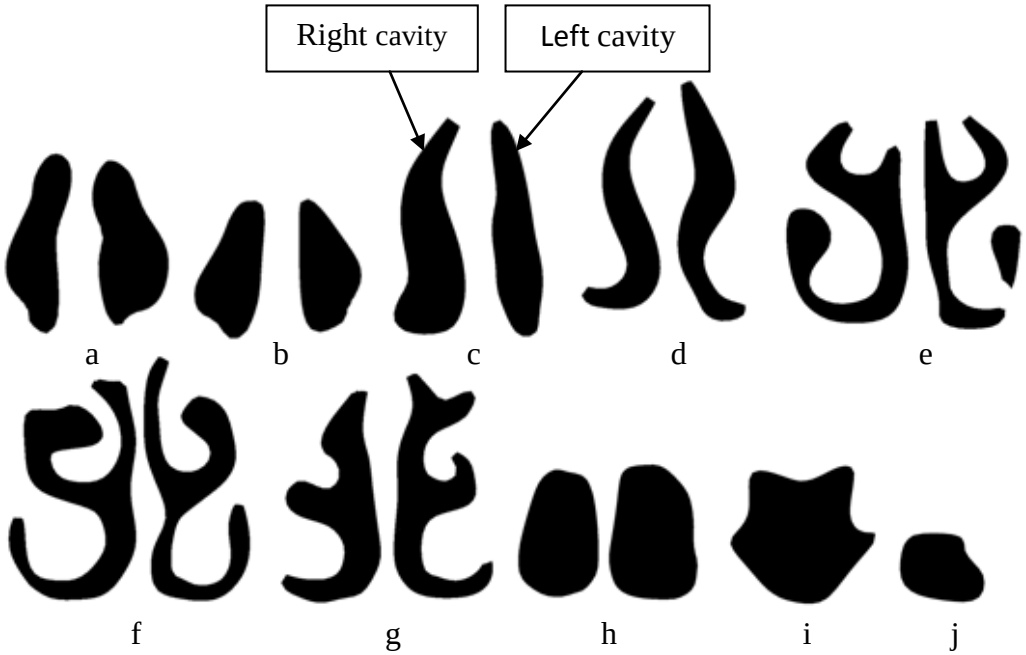

Figure 4.3: Ten cross section area through the nasal cavity

Figure 4.4 shows the cross-sectional area plot of the present computational model compared to the existing data of the male nasal cavity from others published work. In Figure 4.4, it was observed that the cross section area of the left nasal cavity was greater than the right nasal cavity at the most of the location along the nasal cavity. This shows that the nasal cavity is not symmetric and therefore should not be simplified by modelling only one side of the cavity. Also another important observation was the decrease in the cross-sectional area of the female subject when compared to male in the

posterior region. The female nasal cavity is smaller in length (8.5 cm) when compared with the male subjects as determined by Cheng *et al*., (1996) and Wen *et al*., (2008) to be 9.5 cm and 9.7 cm respectively.

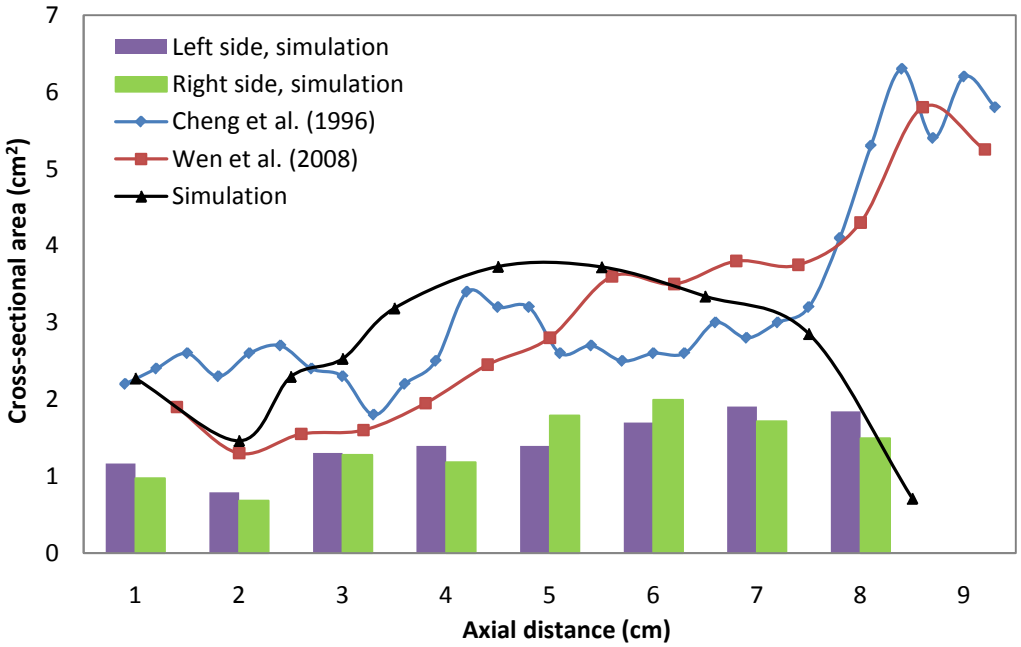

Figure 4.4: The comparison of cross-sectional area vs. axial distance from anterior to the posterior of the nasal cavity

Although inter human differences in nasal anatomy and geometry exist, a general trend can be observed. The smallest cross section area was found at the nasal valve region. The cross section area for the present model is 1.46 cm^2 while 1.9 cm^2 and 1.4 cm^2 for Cheng *et al*., (1996) and Wen *et al*., (2008) respectively. An increase in the cross-sectional profiles was also observed after the nasal valve region. This will cause the inspired airflow reach the olfactory region and at the same time spread the airflow into the inferior, middle and superior turbinate region. For the present geometry, the nasal valve region is located about 2.0 cm from the anterior tip of nose, which compares

with the other models that are located at 3.3 cm and 2.0 cm for Cheng *et al*., (1996) and Wen *et al*., (2008) respectively.

4.4 Model comparison

Figure 4.5 shows the nasal resistance plot for various flow rate obtained from the present computational model compared with the existing data available. The average pressure drop between the nostril and nasopharynx was obtained at flow rates from 7.5L/min to 40 L/min. A laminar model for the flow rates 7.5 to 15 L/min and the SST k-ω turbulent model for the flow rates 20 to 40L/min were used to simulate the flow fields. For the laminar flow rates (<15 L/min) the slope of the impedance curve for our simulation is almost the same as found by other researchers. However, as flow rate increases, turbulence plays a significant role, the impedance curve start to depart from each other as seen in Figure 4.5.

From the observation, the nasal resistance in the case of female model also follows the same pattern as that of the male subject. However the slope of the resistance curves as seen in Figure 4.5 is steeper in case of the female subject. This may be attributed to the anatomical differences; female model is shorter in length and has smaller posterior cross sectional area. At low velocity, the flow is laminar. It was observed that the flow is smooth and properly arranged. Hence, the nasal area is not the critical factor that determines the pressure drop. But when the flow is turbulent, it consists of chaotic, highly disordered flow and also exhibit higher flow speed. Hence the nasal area plays an important role and also results in recirculation and reverse flow. Furthermore, incomparison to the male models, the current female model exhibited

smaller cross sectional area at the nasopharynx. This is also the reason for the current female model to have higher value of pressure drop.

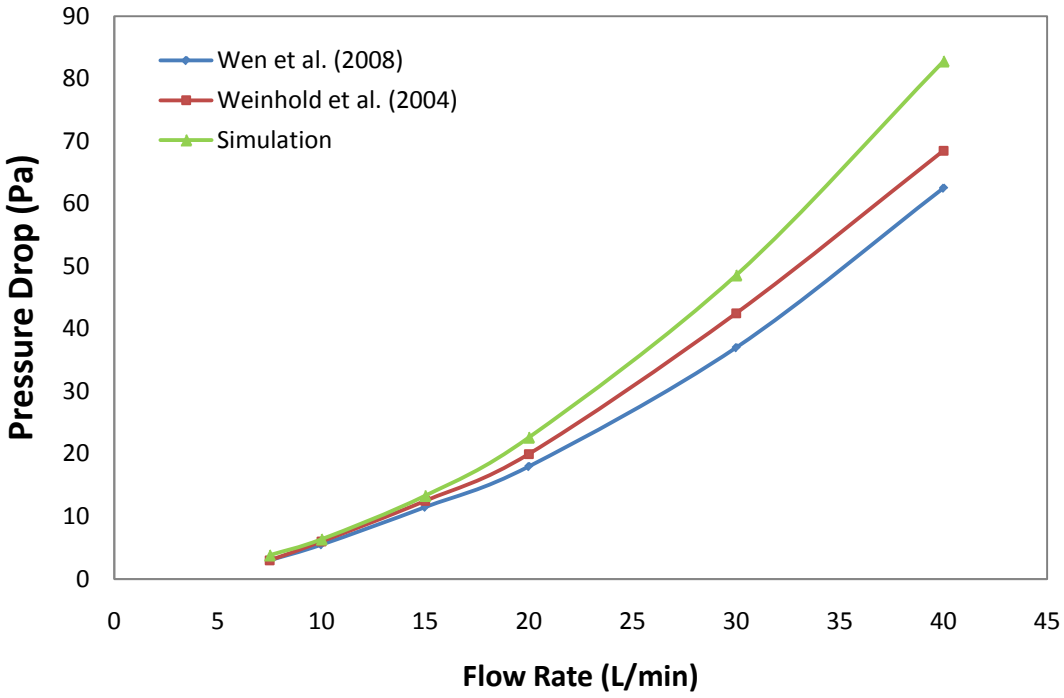

Figure 4.5: Pressure drop vs. inspiratory flow rates compared with previous data

The pressure drop obtained for the female nasal cavity was around 22.6 Pa for 20 L/min when compared with male model at around 18 Pa & 20 Pa for the same flow rate as obtained by Wen *et al*., (2008) and Weinhold *et al*., (2004) respectively. Hence, in spite of the anatomical differences a close resemblance of result can be seen with the respect to the previous studies, thereby validating of our present study.

4.5 Basic flow studies

Understanding the properties of airflow in the nasal cavity is very important in determining the nasal physiology and in diagnosis of various anomalies associated with the nose. However, the conventional methods like rhinomanometer and acoustic rhinometry fail to accurately predict and quantify the flow properties at every location inside the nasal cavity. Airflow simulations based on computational fluid dynamics is most useful for better understanding of flow phenomenon inside the nasal cavity. Hence, in the present study, the numerical simulation of nasal airflow was performed in order to obtained details of flow characteristic along the nasal cavity. This chapter present the results obtained from numerical study of nasal airflow for 20 L/min during inspiration.

4.5.1 Reynolds number calculation

The Reynolds number usually is used to characterize the type of the flow, whether the flow is laminar or turbulent. Reynolds number is a dimensionless number which also present the ratio of inertial forces to viscous forces acting on a fluid element. Reynolds numbers of the nasal airflow can be obtained from:

$$Re = \frac{\rho u d}{\mu} \tag{4.1}$$

Where ρ the air density ($1.225\ kg/m^3$), u is the airflow velocity, d is the diameter of the nasal inlet and μ is the dynamic viscosity of the air ($1.7894 \times 10^{-5}\ kg/ms$). The initial prediction of the Reynolds number value is important in order to properly simulate the nasal airflow. The flow will be defined as laminar for $Re < 2100$ and turbulent for $Re >$

2100. In the present work, numerical simulation were carried out for flow rates of 7.5 L/min, 10 L/min, 15 L/min, 20 L/min, 30 L/min and 40 L/min. The Reynolds number value for flow rates of 1 5L/min calculated from the equation above is 1,597. Based on the Reynolds number obtained, the airflow was treated as laminar for flow rates up to 15 L/min. This was in general agreement with previous researchers (Wen *et al*., 2008; Segal *et al*., 2008) who determined laminar nature of the flow, for flow less than 15 L/min. The Reynolds number obtained for 20 L/min based on the equation above is approximately equal to 2,129. Hence, the flow was treated as turbulent for flow rates of 20 L/min and above.

4.5.2 Velocity

Figure 4.6 shows the contour plot of the average velocity value along the nasal cavity during inspiration. As seen in Figure 4.6, the flow was observed to be fully developed along the middle meatus region. The superior and inferior meatus pathway received lesser flow. Low velocity value was also observed at the inferior and superior turbinate regions. As seen in Figure 4.6 and 4.7, sudden increase of average velocity value was noticed at the nasopharynx region. This is due to decrease in cross section area at the posterior region of the nasal geometry.

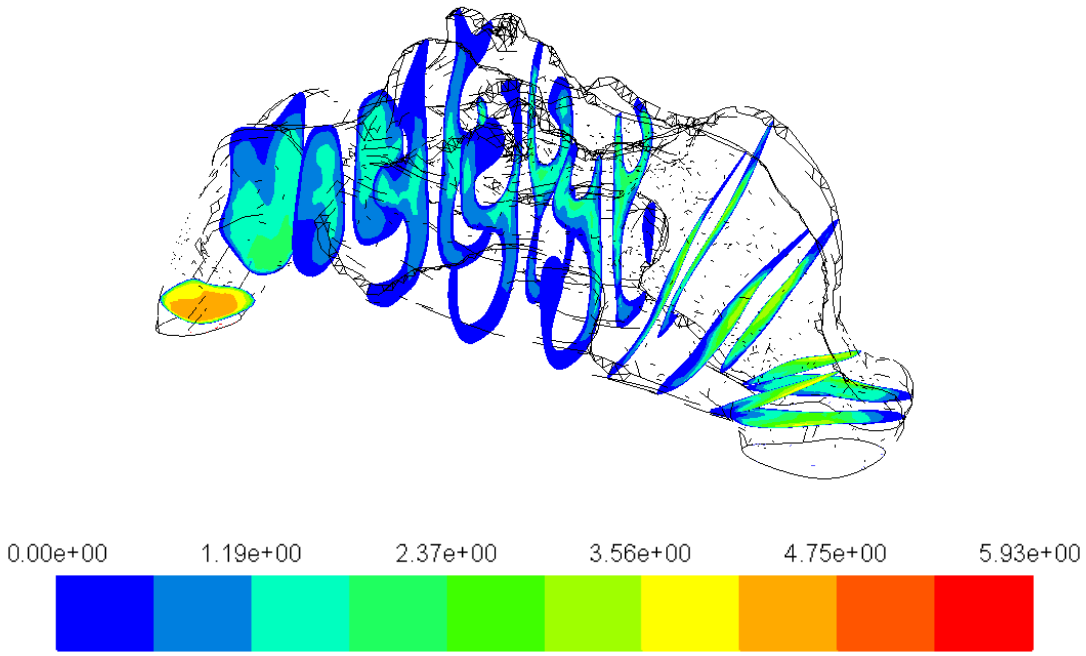

Figure 4.6: Average velocity contour along the nasal cavity

As seen in Figure 4.7, the nasal valve located at a distance of around 2cm from the anterior region of the nasal cavity. The maximum velocity attained at the nasal valve location varies from 4.18 m/s as against 4.82 m/s & 3.1 m/s obtained by Xiong *et al.*, 2008 and Croce *et al.*, 2006 respectively. The peak airspeed in each plane decreases posteriorly beyond nasal valve region as the cross sectional area increase.

Figure 4.8 shows the streamline plot of the inspired nasal flow through the nostril. As seen in Figure 4.8, the low velocity re-circulating stream was found just posterior to the nasal valve region. The re-circulatory flow propagates the flow to the olfactory region thus making contact with the olfactory sensor. The aerodynamic shape of the nasal cavity facilitates the re-circulatory flow caused by adverse pressure gradient due to sudden increase in cross section area after the nasal valve region.

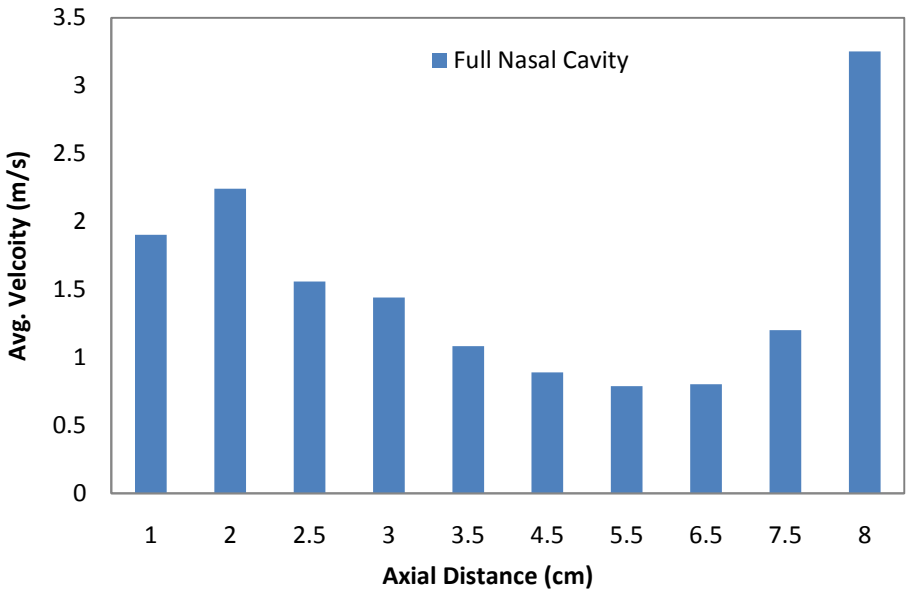

Figure 4.7: Variation of average velocity along the length of the nasal cavity

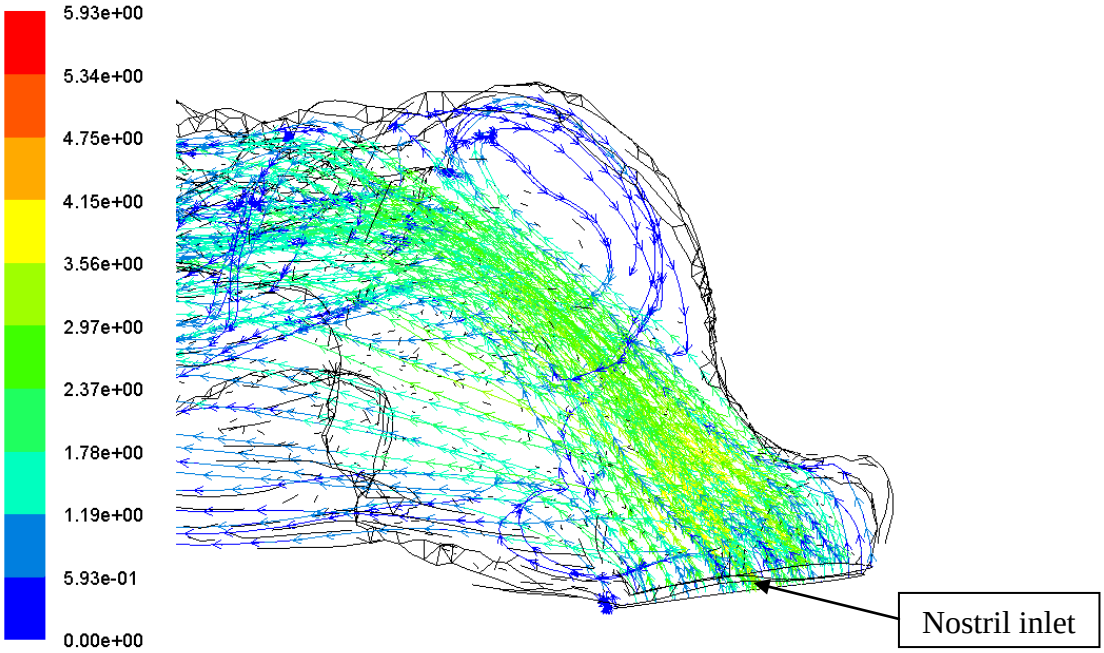

Figure 4.8: Flow recirculation at the olfactory region

As can be seen from Figure 4.9, the velocity in the left cavity is higher than the right cavity. The velocity variation was significant in the anterior region. The result obtained for the left and right side nasal cavity varies due to the non-symmetrical shape of the nasal cavity.

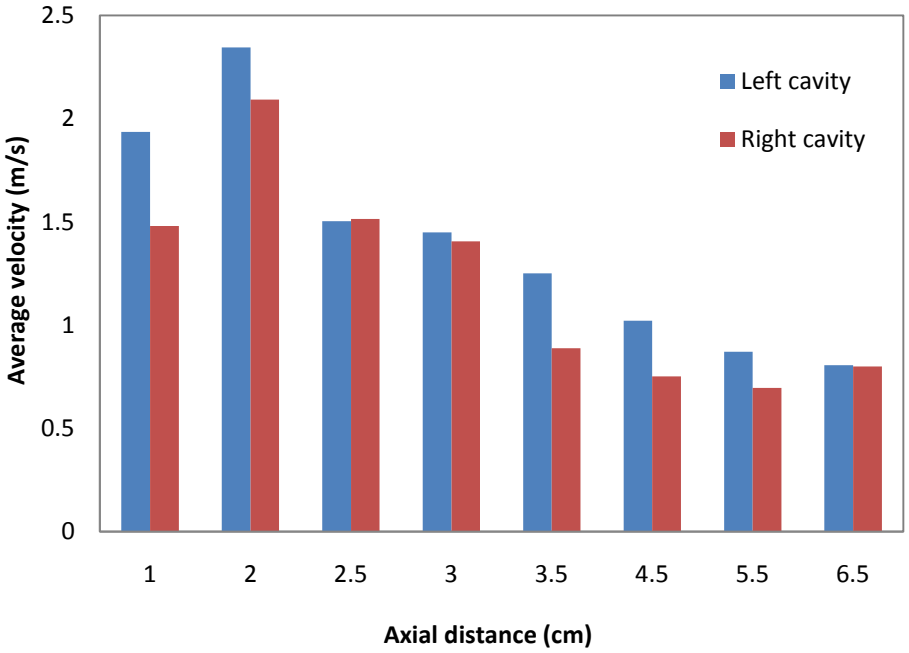

Figure 4.9: Comparison between left and right nasal cavity

4.5.3 Pressure

As shown in Figure 4.10, the average static pressure across each sectional plane decreases along the axial length and remain almost the same for over a length of 2 cm from the nasal valve. Further downstream along the posterior region, the average static pressure value keeps decreasing. It has been found that there is sudden decrease in the average static pressure in the nasopharynx region where a bend is encountered. During

inspiration, the lungs suck in air from the ambient atmosphere. Hence negative pressure profile is observed for the inspiratory flow.

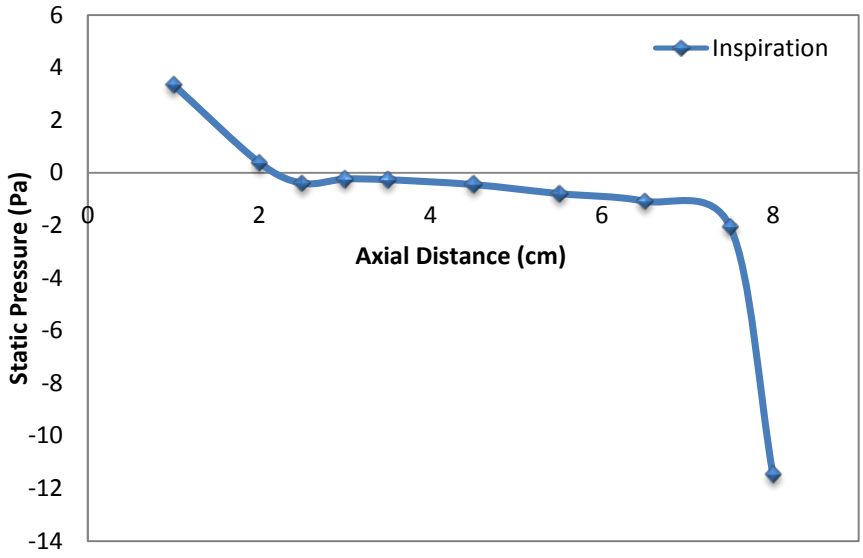

Figure 4.10: Average static pressure along the nasal cavity during inspiration

4.5.4 Wall Shear Stress

Figure 4.11 shows the maximum wall shear stress across various sections along the axial length of the nasal cavity. As seen in Figure 4.11 and Figure 4.12, the highest wall shear stress can be observed at the anterior and the posterior ends. This may be attributed to the sudden change in cross section area at the inlet and outlet. The maximum wall shear stress obtained at the nasal vestibule and nasal valve region is 1.044 Pa and 0.9452 Pa accordingly. The wall shear stress value decrease significantly after the nasal valve region where the velocity decreases. The wall shear stress value can be expressed as

$$\tau_{\omega} = \mu \frac{\partial u}{\partial y} \tag{4.1}$$

where μ is the dynamic viscosity, u is the flow velocity parallel to the wall and y is the distance to the wall. The changes in flow direction at the nasopharynx due to the bend and this result in increased in wall shear stress value at the posterior end. The maximum wall shear stress value obtained at the nasopharynx region approximately equal to 0.8372 Pa.

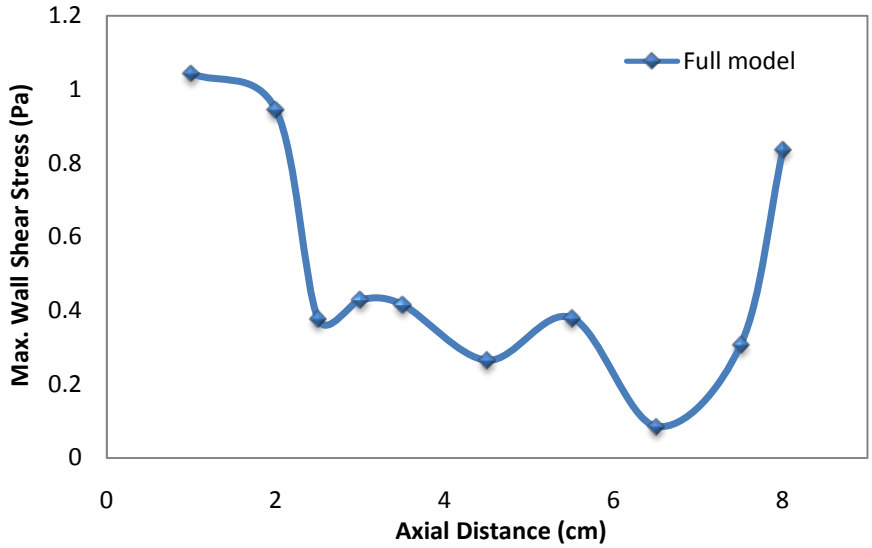

Figure 4.11: Maximum wall shear stress along the axial distance of the nasal cavity (full model)

Figure 4.12 shows the contour plot of the average wall shear stress value through the nasal cavity during inspiration. As seen in Figure 4.12b, the protruding middle turbinate in the left nasal cavity results in the high wall shear stress effect. The geometry of the septum offers resistance to flow at the wall surface and results in the increased wall shear stresses. At the nasal valve where there is sudden increase in velocity due to

its narrow cross- sectional area, hence result in higher value of maximum wall shear stress. The comparison between left and right nasal cavity as indicated by Figure 4.13, shows the prevalence of higher wall shear stresses in the left nasal cavity due to variation in cross section area. The maximum wall shear stress value obtained at the nasal vestibule region for the left nasal cavity is equal to 0.9503 Pa and 0.4013 Pa for the right cavity. At the nasal valve region, the maximum wall shear stress value obtained for the left cavity is 0.9452 Pa and 0.5949 Pa for the right cavity. This is due to the unsymmetrical shape of the nasal cavity and the variation of the wall contour between the left and the right nasal cavity.

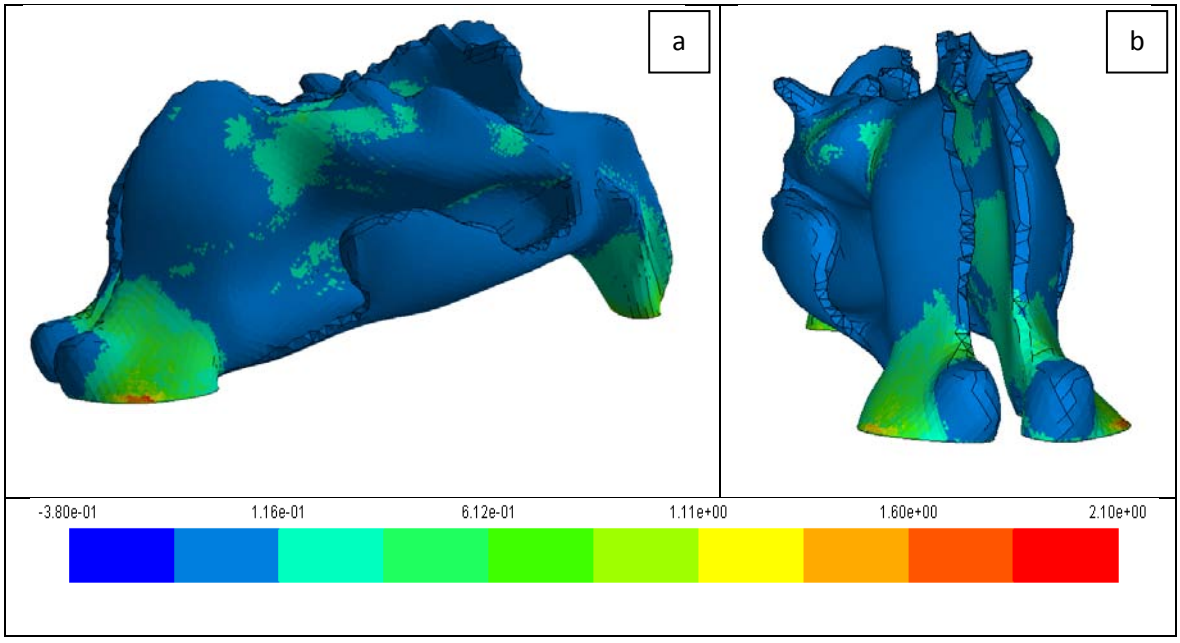

Figure 4.12: Average wall shear stress contour

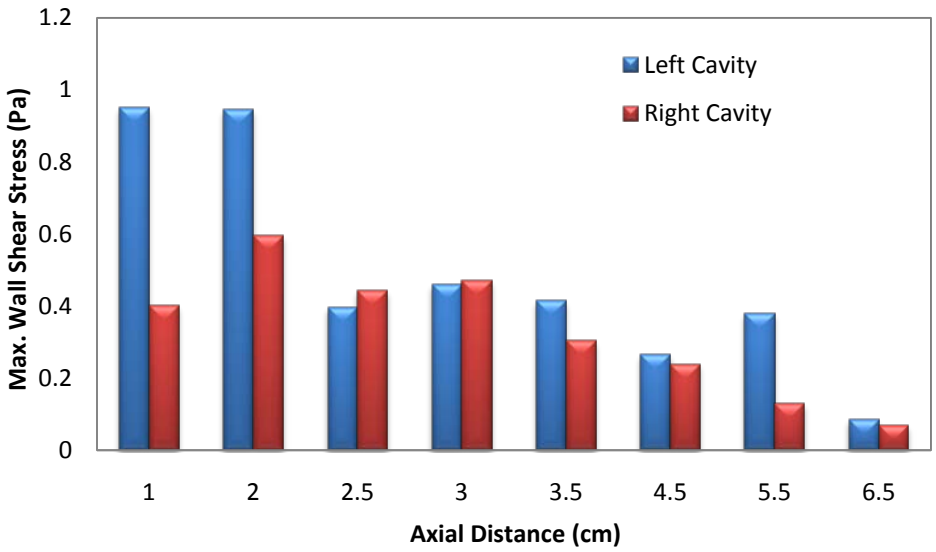

Figure 4.13: Maximum wall shear stress across left and right nasal cavity

4.5.5 Inspiration vs expiration

In this section, the comparative study of the inspiratory and expiratory states have been extensively carried out demonstrating the usefulness of numerical models in better understanding of flow phenomenon inside the nasal cavity and as such should be of benefit to the medical practitioners.

4.5.5.1 Velocity and pressure comparisons

The flow current that enters the nostril during inspiration progresses towards the nasal vestibule with a velocity of around 1.8 m/s. Figure 4.14 shows the variation of velocity along the length of the nasal cavity. The velocity is observed to be higher at the posterior region during expiration when compared with inspiration. Pressure distribution as shown in Figure 4.15 showed marked variations while inspiration and expiration. The

Expiratory mechanism is defined by positive pressure gradients. The flow is thrown out from the lungs and therefore there is prevalence of higher values of pressure during expiration. Whereas inspiration is the mechanism in which the lungs suck the air from the ambient atmosphere. Hence negative pressure profile is observed for the inspiratory flow.

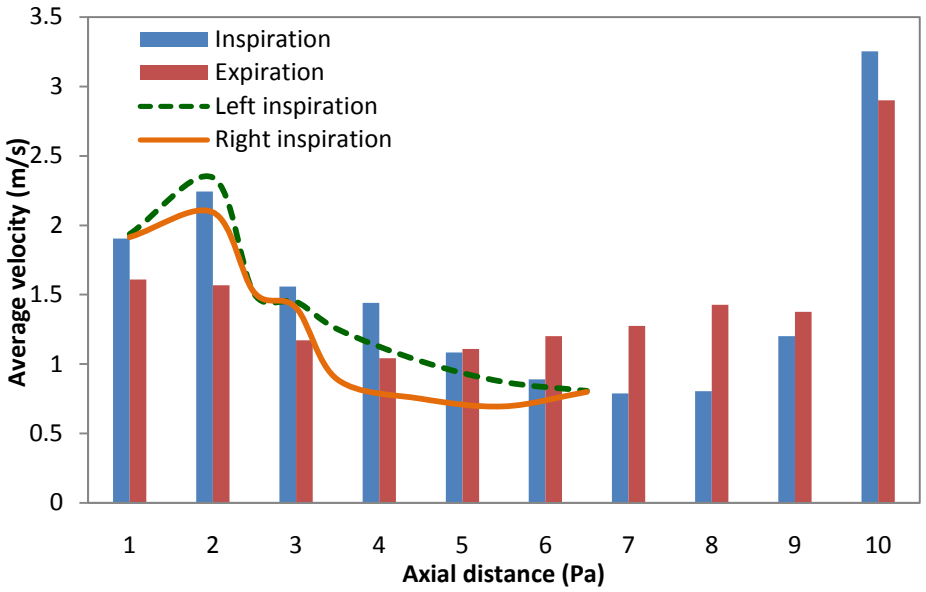

Figure 4.14: Velocity profile comparison during inspiration and expiration

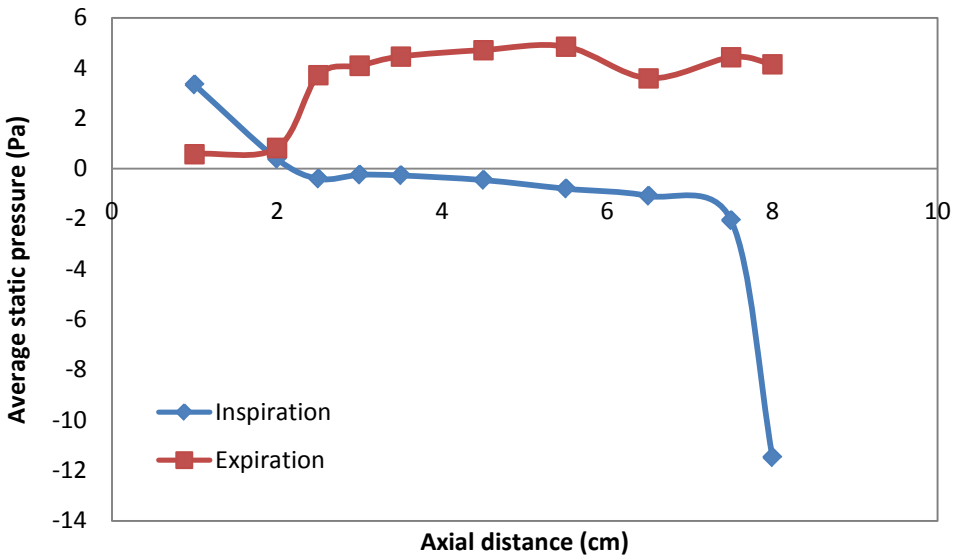

Figure 4.15: Average static pressure along the axial length of the nasal cavity

4.5.5.2 Resistance

Different resistance plots are obtained for inspiration and expiration, indicating the variation of resistance in both processes (see Figure 4.16). Lower resistance values are obtained on expiration when compared to inspiration. There is ambiguity with respect to observations on resistance during inspiration and expiration. Haight and Cole, (1983) noted that during quiet respiration the resistance to airflow was higher during inspiration when compared with expiration. However Kenyon, (1987) observed the opposite and found the expiratory resistance to be higher than the inspiratory one. Viani *et al*., (1990) found the expiratory resistance to be higher when measured at a pressure gradient of 150 Pa.

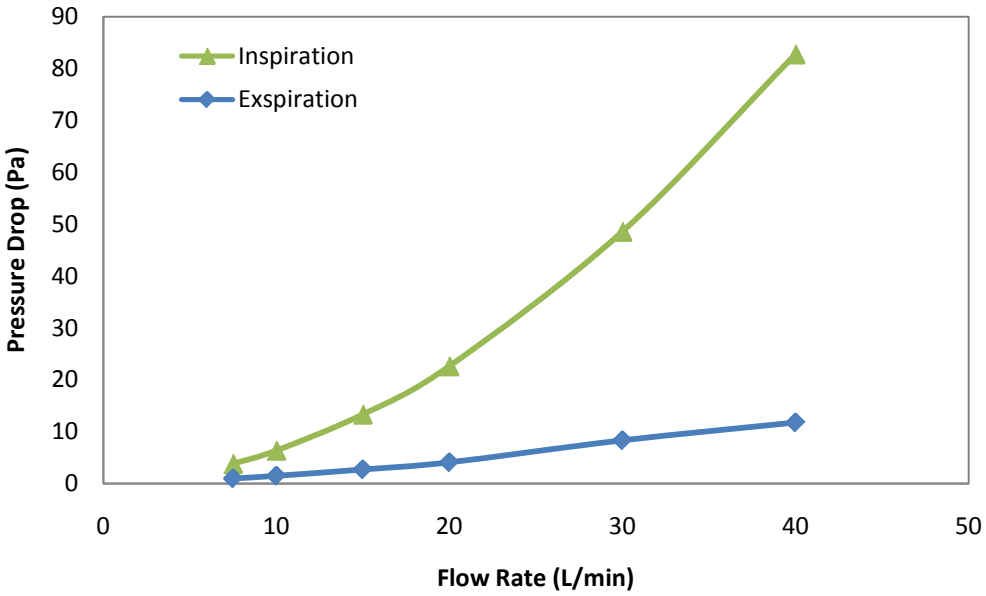

Figure 4.16: Pressure drop value during inspiration and expiration for various flow rates

However the situation was reversed for low flow rates, with the inspiratory flow demonstrating lesser resistance than the expiratory one. Further studies need to be performed to ascertain the current simulated observation. Since the present simulation study does not take into account the collapse of the nasal vestibule from the negative pressures generated during inspiration, the results obtained might not be actual physiological observations.

4.5.5.3 Wall shear stress

The wall shear stresses obtained during inspiratory phase were predominantly higher at anterior region. The maximum wall shear stress obtained at the nasal valve was around 0.97 Pa. The expiratory phase showed much higher values of wall shear stress at the posterior region (Figure 4.17). In summary the expiratory phase results in higher

stress compared with the inspiratory phase. It can therefore be inferred that the high velocity jet expelled during sneezing much higher values of stress having adverse effect on the nasal wall. Continuous sneezing phenomenon may damage the nasal valve and destroy the cell lining and blood vessels attached to walls. However, to the author knowledge, there is no work have quantified the wall shear stress value that could damage the soft tissue and rupture the blood vessel on the nasal cavity.

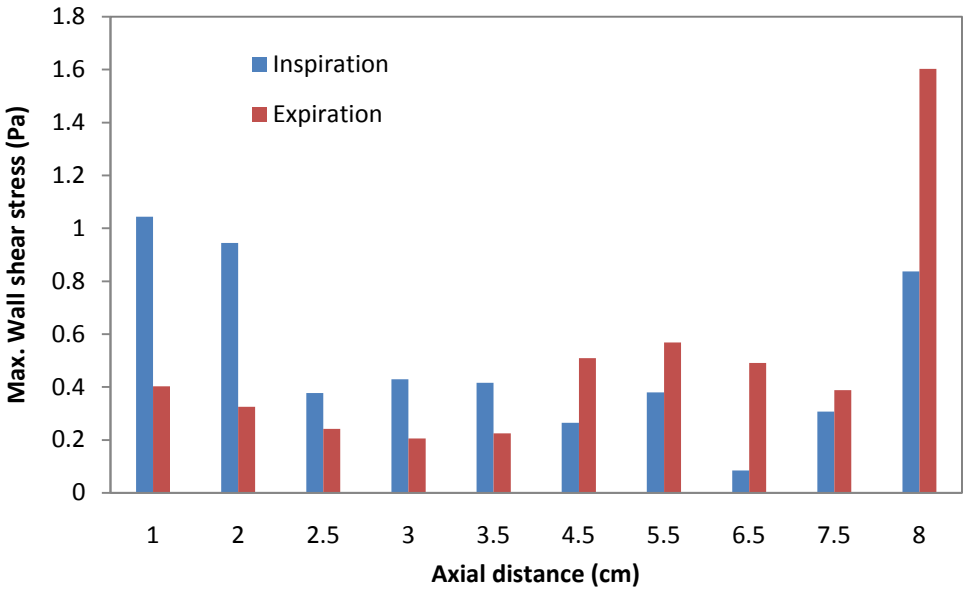

Figure 4.17: Maximum wall shear stress along the axial distance of the nasal cavity

4.6 Various breathing rates for inspiration and expiration

Humans exhibit different breathing rate under different conditions. While sleeping humans tend to have low breathing flow rates then while working or being awake. The normal breathing approaches 20 L/min. Under heavy exercise or while running, the flow rate may increase beyond 40 L/min. Therefore it would be useful to understand the effect of different breathing flow rates on the nasal cavity. In this section, the flow characteristics inside a female nasal cavity has been evaluated using CFD for steady state flow consisting of flow rates varying from 7.5 to 40 L/min in both inspiration and expiration mechanism.

4.6.1 Average velocity

The average velocity values have been extracted for both inspiration and expiration at some important location like the vestibule, nasal valve and the nasopharynx. Figure 4.18 shows the average velocity values for flow rates from 7.5 to 40 L/min obtained at different sections along the nasal cavity during inspiration. As seen in Figure 4.18, irrespective of the flow rates, the highest value of average velocity appears at the nasal valve region during inspiration. Under laminar flow rate ranging from 7.5 to 15 L/min, increment of 7.5 L/min, the average velocity value increased by about 120 %. However, under turbulent conditions having flow rate ranging from 20 to 40 L/min, for an increment of 20 L/min, the difference in average velocity was only about115 %. The maximum velocity at the nasal valve region for the flow rates of 7.5 L/min was 1.54 m/s, which increased to 8.66 m/s for flow rate of 40 L/min. Higher values of velocity at the

nasal valve is detrimental to the health of the tissues and can potentially damage the blood vessels located in that region.

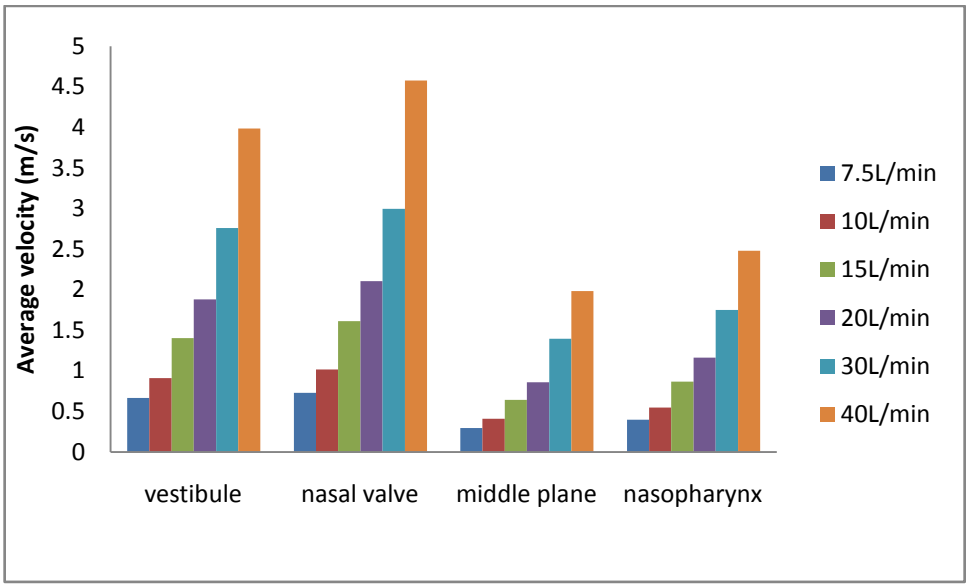

Figure 4.18: Average velocity at different flow rates from 7.5 to 40L/min during inspiration

The impact of varying flow rates at the olfactory region is also presented. At 7.5 L/min, only 0.001 % of the total flow reaches the olfactory region. The Figure 4.19 shows the plane location beyond which the olfactory region is located. Olfactory region receives only a small percentage of the total flow that enters the nasal cavity. This re-circulatory flow which is composed of very low velocity is useful for the olfactory sense perception. The average velocity for a flow rate of 7.5 L/min was as low as 0.089 m/s. However, as the flow rate increased to 40 L/min, the percentage of flow that reached the olfactory sensors also increased to 0.28 % of the total flow. When a large flux of air reaches the olfactory sensors, the average velocity at the region also increased to 1.02 m/s. This explain why when we tend to inhale higher mass flow rate during sniffing, the

perception of smell also improves. Studies by Mullins (1955) and Schneider *et al*., (1963) also have shown that an increase in flow rate increases odor detectability.

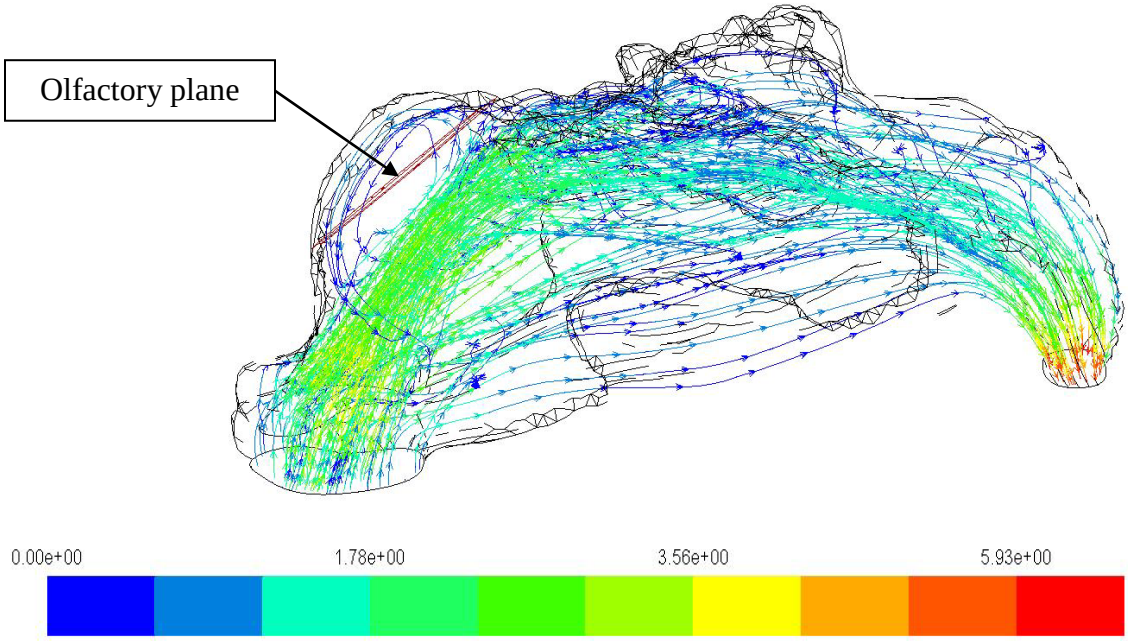

Figure 4.19: Model of the nasal cavity showing the olfactory plane

However, for expiration, the average velocity value attained at vestibule and nasal valve region is almost the same as the flow increase from 7.5 to 40 L/min. In contrast to inspiration, almost uniform velocity profiles can be observed at all locations under lower flow rates. As shown in Figure 4.20, only marginal variations were observed between various locations as the flow rate increased.

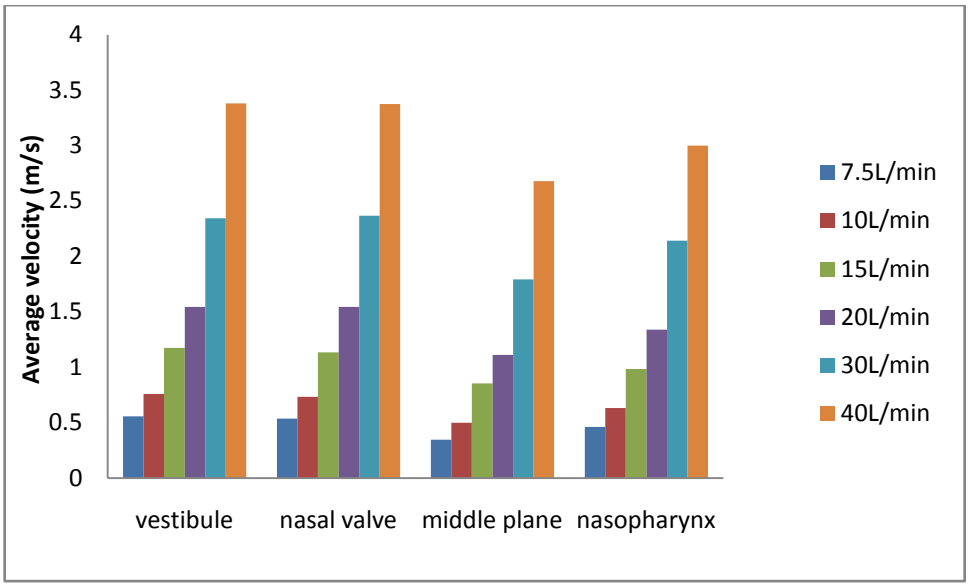

Figure 4.20: Average velocity at different flow rates from 7.5 to 40L/min during expiration.

4.6.2 Wall shear stress

Figure 4.21 and 4.22 shows the plot of maximum wall shear stresses for inspiration and expiration. Figure 4.21 shows the impact of increased flow on the wall shear stress value through the nasal cavity. The impact of high velocity with the increased flow rate is predominant at the anterior region in case of inspiration. The value of maximum wall shear stress at the vestibule region increased by more than 2000 % as the flow rate increased from 7.5 to 40 L/min. Such an abrupt increase has significant impact on blood vessels in the region. However, expiration demonstrated near uniform prevalence of wall shear stress at almost all locations within the nasal cavity. At the nasal valve and vestibule region, the stress developed during expiration was much lesser than that obtained during inspiration. The value of maximum wall shear stress at the vestibule was around 2.92 Pa when compared to 6.89 Pa for the same location during

inspiration. Therefore the sneezing phenomenon, which is characterized by abrupt and very high expiratory flow rates of greater than 40 L/min, will produce significantly lower wall shear stresses than for the same flow rate during inspiration. Hence even though sneezing is a sudden jet of flow with high velocity, the stresses produced will be much lesser. However, higher flow rates are not desired, since they result in very high values of pressure gradients which may result in the collapse of the nasal vestibule as well induce more stresses in the nasal cavity thereby damaging the delicate tissue layers and blood vessels creating complications.

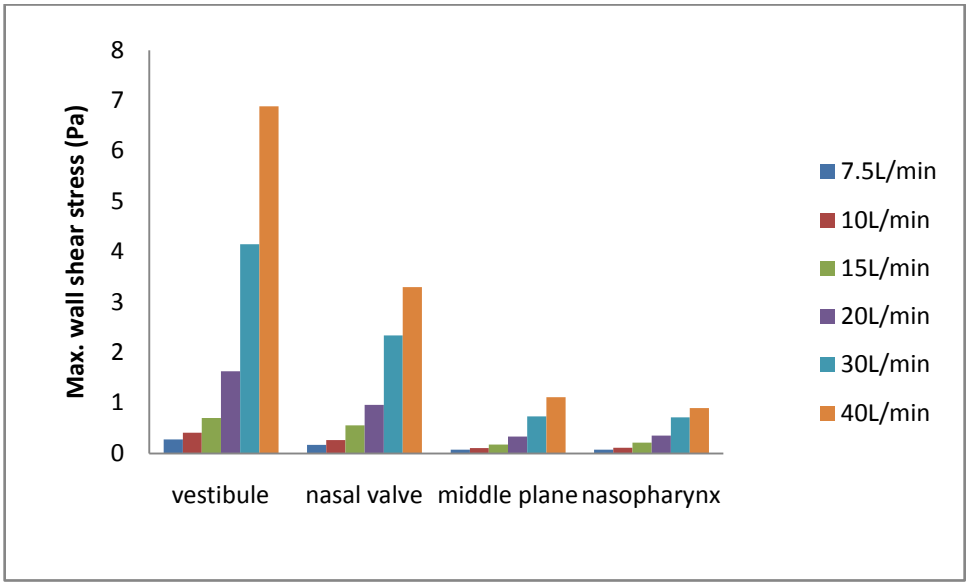

Figure 4.21: Maximum wall shear stress values through the axial distance of the nasal cavity during inspiration

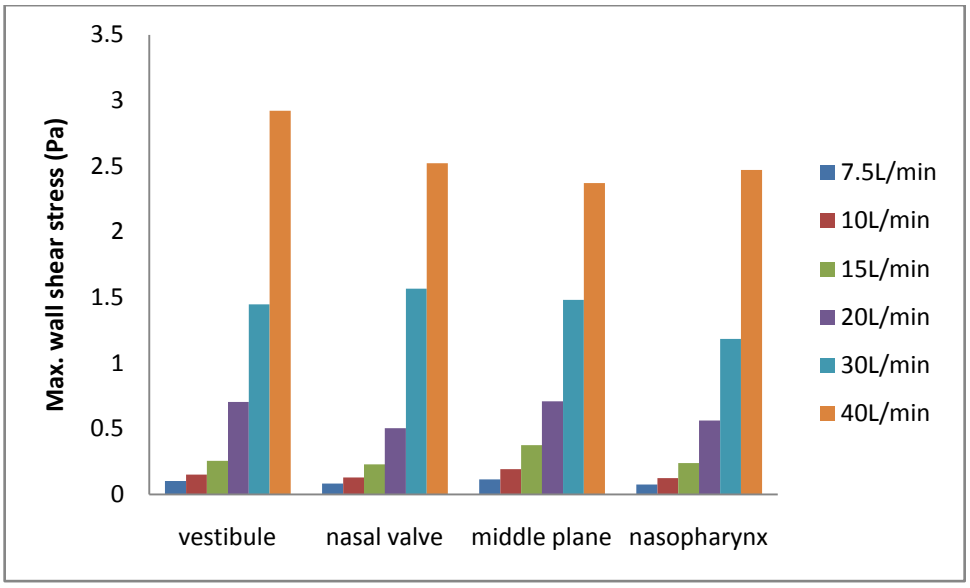

Figure 4.22: Maximum wall shear stress values through the axial distance of the nasal cavity during expiration

4.7 Preliminary work on gender comparison

Evidence suggests that there is no gender difference in upper airway size whether measured directly by imaging methods or indirectly by measurement of upper airway resistance. (Rowley *et al*, 2001). However some of the problems like obstructive sleep apnea are specific to only males (Suzina *et al*., 2003). The anatomical variations contribute to gender based occurrence of certain anomalies. Hence gender is one of the contributing factors for the difference in the flow behavior.

4.7.1 Geometry comparison

In order to verify the anatomical differences based on gender, the length of the nasal cavity was measured from a sample of available CT images. As a result a sample of 4 cases each of male and female CT nasal images were measured. Table 4.1 shows the total length of the nasal cavity obtained from the CT scan images of four male and four female human subjects. It was found that the female models were slightly smaller in length when compared to the male models. Based on the results shown in Table 4.1, we can conclude that female have shorter length of nasal cavity when compared to their male counterparts. However, this is just sample evidence which need to be corroborated with much higher samples to verify the observations reported in Table 4.1.

Table 4.1: The total length of the nasal cavity based on the gender comparison

Name	Length (mm)
Female 1	85.72
Female 2	89.78
Female 3	88.90
Female 4	90.97
Male 1	96.69
Male 2	91.73
Male 3	98.48
Male 4	97.37

The current work is focussed on computational study of nasal cavity, hence in order to further the understanding of the effect of gender based anatomical differences on the flow behaviour; numerical analysis has been carried out. Most of previous works on numerical studies of nasal cavity based their observation on male models while the current research is using female models that developed from CT images.

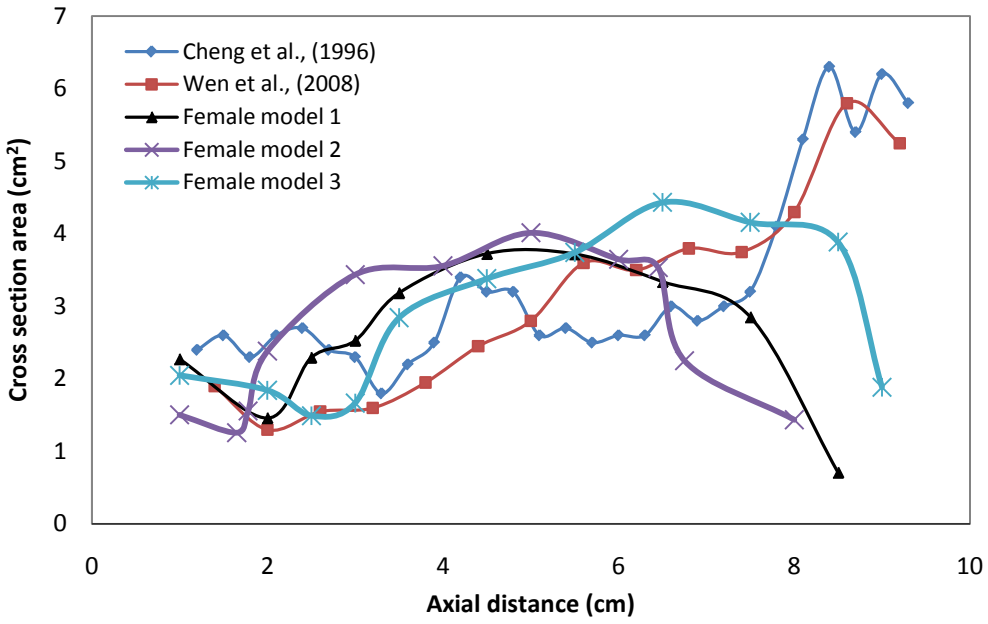

Figure 4.23: The comparison of cross section area through the nasal cavity of the human male and female subjects

Figure 4.23 shows the cross section area obtained based on the planes created across the nasal cavity. The female computational models are compared with the available male nasal cavity models from the previous published works. As seen in Figure 4.23, the total length of the nasal cavity for female subjects is shorter compared to the male model developed by Cheng *et al*., 1996 and Wen *et al*., 2008. The location of the nasal valve region also varied for each nasal model. Irrespective of gender this difference in location has also been reported in previous literature (Keyhani *et al*., 1995, Subramanium *et al*., 1998, Cheng *et al*., 1996). It also can be observed that the cross section area at the turbinate region for the female nasal cavity is wider compared to male. As seen in Figure 4.23, at the posterior region of the nasal airway, a substantial increase in cross section area was observed after the turbinate region for male. Conversely, the cross section area of the female nasal airway decreased drastically after the turbinate region. Thus it was observed that the female possessed smaller cross section area at nasopharynx. The cross section area at the nasopharynx is 5.8 cm^2 and 5.25 cm^2 for male and 2.85 cm^2, 3.52 cm^2 and 2.96 cm^2 for female nasal cavity. Thus the female nasal cavity is shorter in length and has smaller posterior cross sectional area.

The nasal resistance in the case of female model also follows the same pattern as that of the male subject for laminar flow conditions. However under turbulent conditions, resistance curves as seen in Figure 4.24 is steeper. There are significant differences in the values of pressure drop obtained for all the 3 female models. Model 1 exhibited higher values of resistance compared to the male model. The value of resistance for female case 2 was much lesser than that of the male model and the female case 1. Also the female case 3 showed lower values of resistance than its male counterparts.

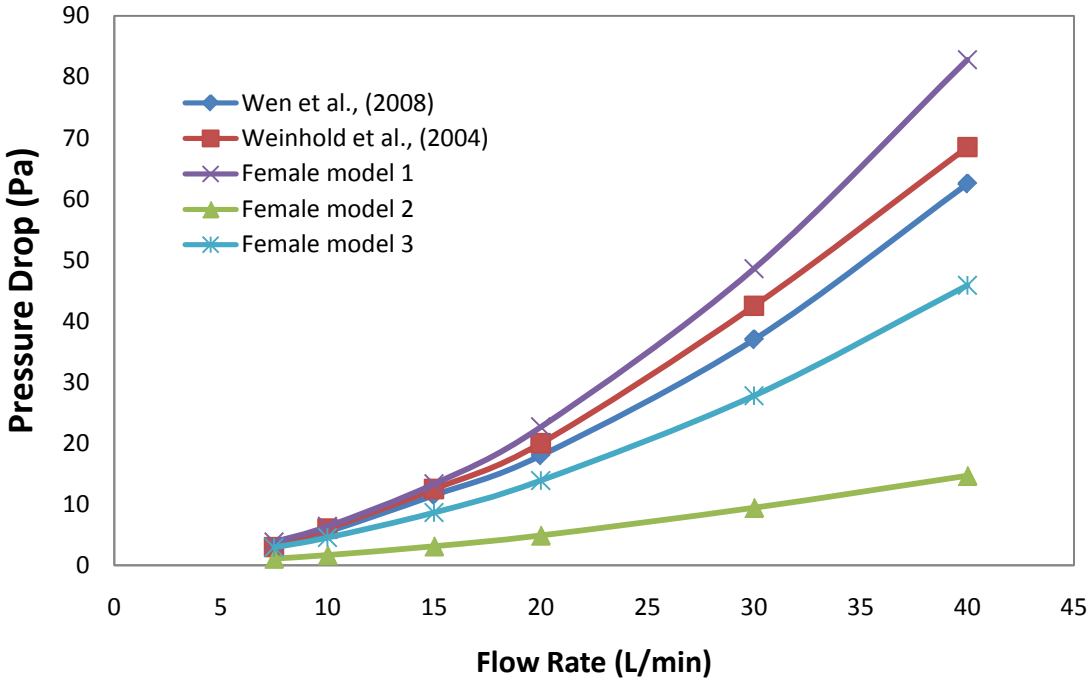

Figure 4.24: the pressure drop value across the nasal cavity

These variations in values for the three processed female case studies maybe attributed to the inter-human anatomical differences that exist between humans. Secondly, the values of resistance for the female case 1 having higher values of resistance maybe due to artifacts associated with the model itself. Also the female case 1 had the smallest cross section area at the nasopharnyx outlet which may contribute to the increased resistance. In general, the female model displayed lower values of pressure drop when compared with the male models.

A gender based study is carried out as observed in Table 4.2. Four male nasal cavity models from previous publications were considered for the current study on the basis of data available in the literature. Most of the researchers used male subjects to determine the nasal patency (Wen *et al*., 2008; Weinhold *et al*., 2004; Cheng *et al*., 1996, Subramaniam *et al*., 1998).

Table 4.2: Characteristic description of nasal cavity for male and female nasal cavity models

Particulars	**Male**	**Female**
Total length of the nasal cavity	9.2 cm (Wen *et al*., 2008) 9.3 cm (Cheng *et al*., 1996)	8.5 cm (Model 1) 8.0 cm (Model 2) 9.0 cm (Model 3)
Nasapharynx cross sectional area	5.25 cm^2 (Wen *et al*., 2008) 5.8 cm^2 (Cheng *et al*., 1996)	2.85 cm^2 (Model 1) 3.52 cm^2 (Model 2) 2.96 cm^2 (Model 3)
The location of the nasal valve region	3.3 cm (Cheng *et al*., 1996) 2.0 cm (Wen *et al*., 2008)	2.0 cm (Model 1) 1.65 cm (Model 2) 2.0 cm (Model 3)
Nasal valve cross section area	1.4 cm^2 (Wen *et al*., 2008) 1.8 cm^2 (Cheng *et al*., 1996)	1.5 cm^2 (Model 1) 1.26 cm^2 (Model 2) 1.84 cm^2 (Model 3)
Pressure drop (for flow rate of 20L/min)	18 Pa (Wen *et al*., 2008) 20 Pa (Weinhold *et al*., 2004)	22.6 Pa (Model 1) 4.88 Pa (Model 2) 13.88Pa (Model 3)
Maximum velocity at nasal valve (for flow rate of 15L/min)	4.2 m/s (Subramaniam *et al*., 1998)	3.17 m/s (Model 1) 2.68 m/s (Model 2) 2.23 m/s (Model 3)

As seen in Table 4.2, the female model has shorter length of nasal cavity (8.5 cm, 8 cm and 9 cm) when compared with that of the male subjects as determined by Cheng *et al*., (1996) and Wen *et al*., (2008) to be 9.3 cm and 9.2 cm respectively. Also another important observation was the decrease in the cross-sectional area of the female subject when compare to male in the posterior region. The nasopharynx cross section area

obtained for this study was 2.85 cm^2, 3.52 cm^2 and 2.96 cm^2; while 5.25 cm^2 and 5.8 cm^2 was determined by Wen *et al*., (2008) and Cheng *et al*., (1996) respectively. This clearly indicated that the male nasal cavity had larger posterior cross sectional area, emphasising the variation based on gender.

Although we do find anatomical variation between male and the female model, a general trend can be observed. An increase in the cross-sectional profiles was observed after the nasal valve region. For the present geometry, the nasal valve region was located about 2.0 cm, 1.65 cm and 2 cm from the anterior tip of nose, which compares with the other models that were located at 3.3 cm and 2.0 cm as obtained by Cheng *et al*., (1996) and Wen *et al*., (2008) respectively. As stated earlier, irrespective of gender, the difference in location has also been reported in previous literature (Keyhani *et al*., 1995, Subramanium *et al*., 1995, Cheng *et al*., 1996).

One of the advantages of using CFD is its accurate presentation of the physiological function associated with the nasal cavity. It presents useful quantification between the male and the female physiological function. The pressure drop at 20 L/min obtained for the female nasal cavities was 22.6 Pa for model 1, 4.8 Pa for model 2, and 13.88 Pa for model 3 when compared with male model at around 18 Pa & 20 Pa for the same flow rate obtained by Wen *et al*., (2008) and Weinhold *et al*., (2004) respectively. The female model 1 had the smallest cross section area at the nasopharnyx outlet hence the higher value of pressure drop was obtained in comparison to model 2 and model 3. However, in general the value of pressure drop for female case 2 and 3 is lower than the male models reported in the literature.

Nasal valve being the critical area of the nasal cavity, comparison between the male and female models resulted in the female models exhibiting lesser value of

maximum velocity when compared with the male model developed by Subramanian *et al*., 1998 the value of maximum velocity obtained for the three female models are 3.17 m/s, 2.68 m/s, and 2.23 m/s respectively as against 4.2m/s for similar flow rate obtained for the male model. This shows the relative difference between the male and the female flow behaviour.

The current study has identified certain gender based anatomical and physiological differences. The use of computational fluid dynamic has assisted in the understanding of these differences which could not be earlier quantified based on mere medical observation and devices. Also, it has highlighted the fact that numerical models cannot be generalized for quantification because gender based differences exists. Hence in all the future numerical study of flow through the nasal cavity, it is imperative to mention the gender of the model under consideration.

4.8 Gravity effect on nasal airflow due to the change of posture

The influence of postural changes in nasal cavity has been investigated in this section. Many reasons have been cited for the increase in the nasal resistance, from increase in the central venous pressure resulting in congestion of the nasal mucosa, also pressing of some of the body areas result in the change in nasal resistance (Roithmann *et al*., 2005). Hence the posture change is an important determinant of upper airway dimensions. The aggravating effect of the supine body position on breathing abnormalities during sleep is attributed to the effect of gravity on the upper airway (Oksenberg and Silverberg, 1998).

Several medical literatures cite the changes in variation in the pharyngeal area with change in posture. But due to the difficulty involved in obtaining CT scan of the person in sitting posture, the CT data obtained in the supine position is utilized to study the effect of posture on the flow. Therefore, this study assumes no changes in the dimension of the nasal cavity with the change in posture. However, the change in the direction of the gravity force acts based on the change of posture is considered for this study. Four cases namely sitting, supine, prone and recumbence right are considered. The acceleration due to gravity is taken to be 9.81 m/s^2 at sea level. The body force weighted pressure discretization scheme is adopted in the numerical simulation where the discontinuity of explicit body forces (e.g. gravity, swirl) was taking into account.

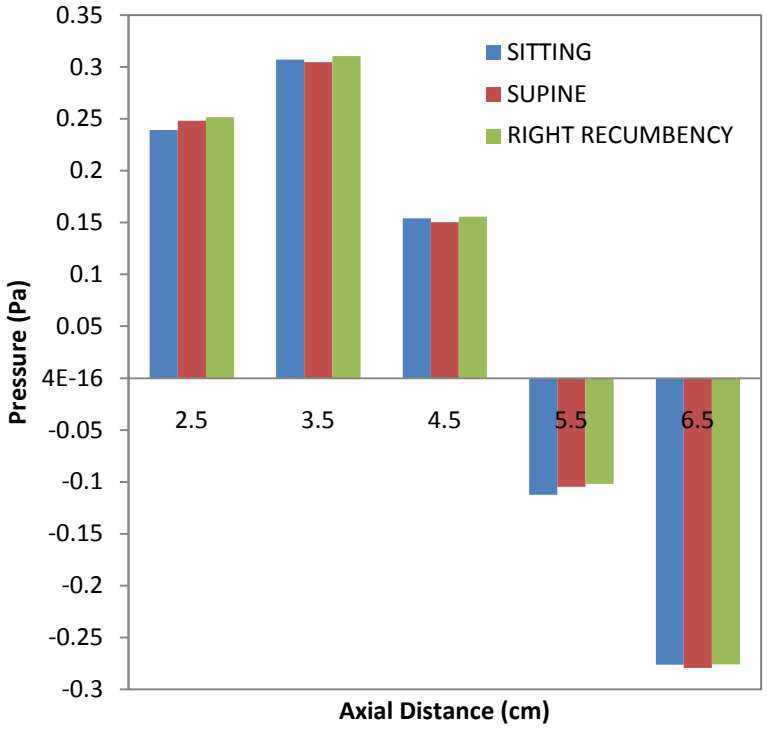

Figure 4.25: Variation of Average static pressure with posture

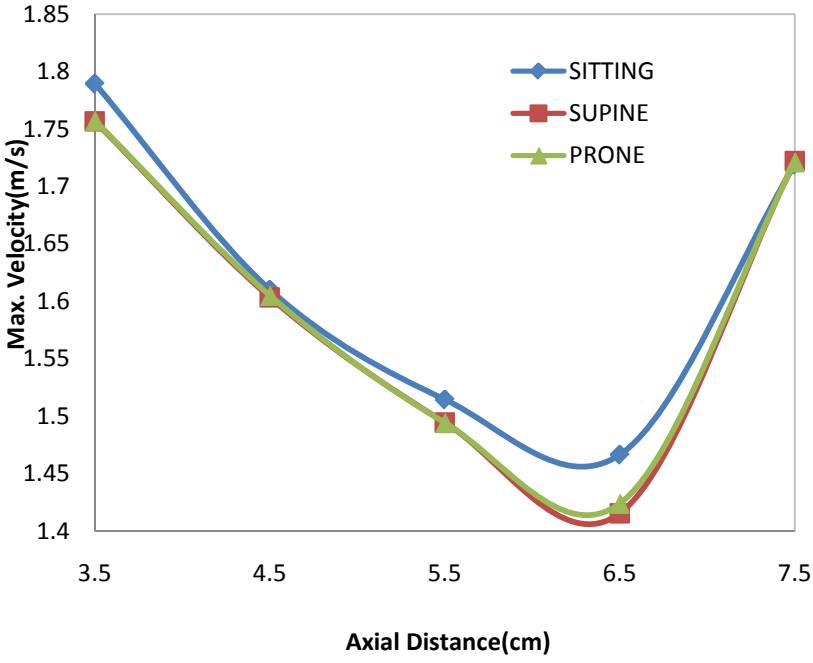

Figure 4.26: Effect of change of posture on velocity at 15L/min

As seen from the Figure 4.25, around 0.3 % change in the average static pressure is observed while changing from sitting to supine position. Along the middle region the average static pressure decreases as we change position from sitting to supine. Also significant changes were observed on shifting to right recumbency position. These results show the influence of gravity associated with the change in posture.

Figure 4.26 shows the variation in the maximum velocity beyond the nasal valve region (3.5 cm to 7.5 cm). Significant drop in velocity can be seen while shifting from sitting to supine position. Not much variation in velocity was observed between the supine and the prone position.

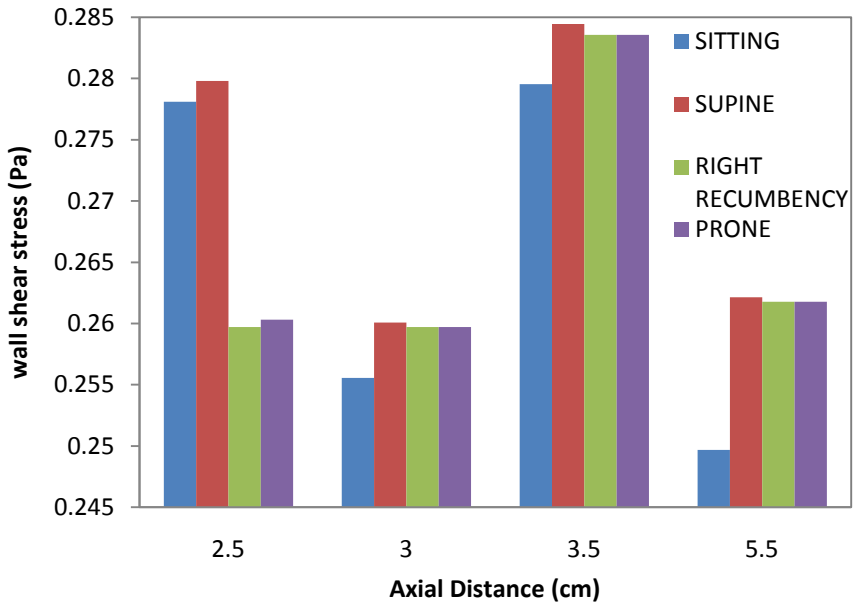

Figure 4.27: Variation in maximum wall shear stresses with change of posture

Also the change in posture had significant effect on the wall shear stresses as can be observed from Figure 4.27. The contours shown in Figure 4.28, shows the effect of change of posture on the flow separation. We can observe that the flow along the right

nasal cavity decreases when changing posture from sitting to supine. The flow is fully developed in the right nasal cavity in sitting position (Figure 4.28A) in comparison with the supine posture.

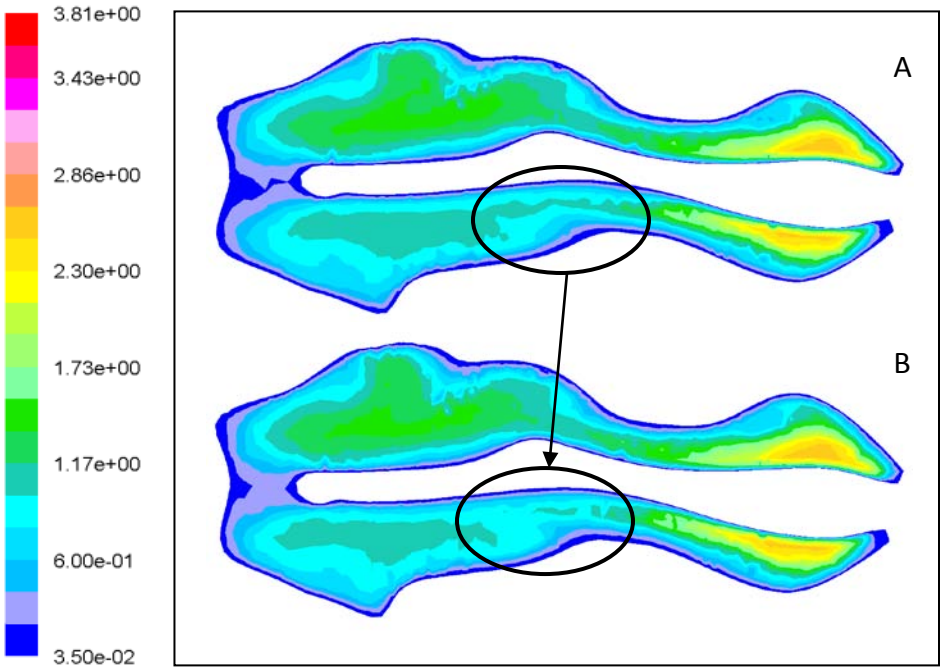

Figure 4.28: A: Sitting B: Supine, shows flow variations along a horizontal plane at middle meatus region

4.9 Effect of different boundary condition on flow parameters

The authors investigate the effect of various boundary conditions classified as plug flow for boundary values defined at nostril inlet and pull flow which simulates the natural physiological breathing conditions with boundary defined at nasopharynx.

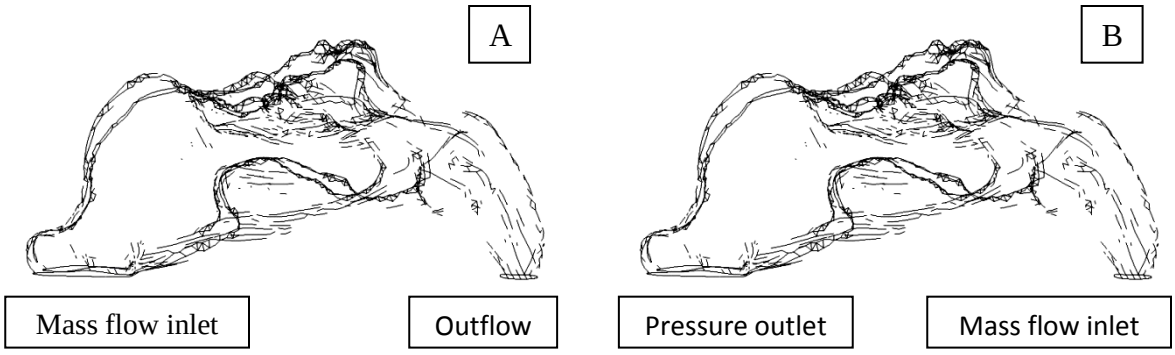

Figure 4.29: Plug flow boundary condition for inspiration A and expiration B

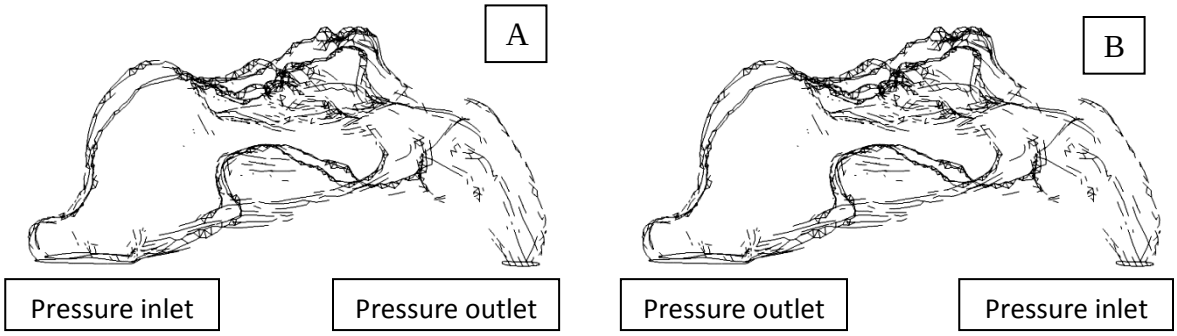

Figure 4.30: Pull flow boundary condition for inspiration A and expiration B.

Inspiratory steady airflow numerical simulations were carried out using 3D nasal cavity model derived from tomography scan images. Figures 4.29 and 4.30 show the plug and pull flow boundary condition definition for inspiration and expiration. Plug and pull flow boundary conditions were employed on the same model and compared to evaluate the effect of different boundary conditions on the flow parameters. Studies are carried out

for various flow rates of 7.5 L/min, 10 L/min, 15 L/min, 20 L/min, 30 L/min and 40 L/min suggesting various breathing rates.

4.9.1 Nasal Resistance comparison for plug-flow and pull-flow

Numerical methods are subjected to various assumptions especially with respect to boundary definition. In order to acquire a more realistic value of nasal resistance, comparative study is performed to understand the effect of boundary condition on the values of resistance determined. Figure 4.31 gives the plot of pressure drop across nasal airway for different flow rates. The pressure drop value increases as the flow rate increases in both cases. The plug flow condition produced substantially high value of pressure drop when compared to pull flow boundary condition. Beyond 20 L/min the pressure drop value increased more drastically for plug flow.

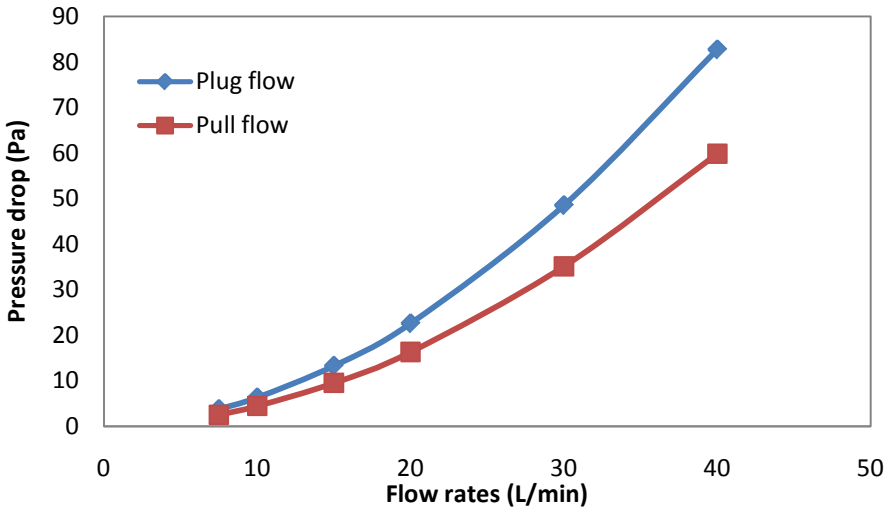

Figure 4.31: Nasal Resistance for different airflow rate

It can be observed that the differences between plug flow and pull flow for inspiration is quite large as observed in Figure 4.32. At the nasal valve, the resistance for plug flow was 0.311 Pa-min/L and for pull flow the value was 0.147 Pa-min/L. Maximum variation was noticed at the vestibule region with 0.3578 Pa-min/L.

In case of the plug flow, the air is forced through the nostrils into the nasal cavity. This explains the prevalence of higher values of pressure drop and nasal resistance in case of the plug flow boundary condition. Hence, it is clear from the pressure drop and the resistance plots that different boundary condition result in variation in flow properties. Therefore, it is very important to adopt the most appropriate boundary condition to evaluate the nasal physiology.

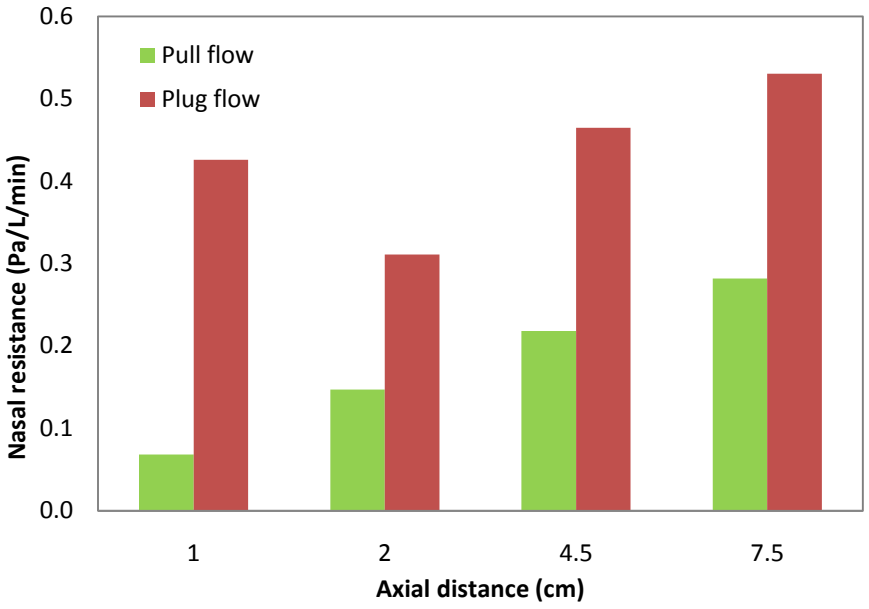

Figure 4.32: Inspiratory nasal resistance for 15 L/min at vestibule, nasal valve, middle section and nasopharynx.

4.9.2 Velocity

Figure 4.33 shows the effect of different boundary condition on velocity along the length of the nasal cavity. Since it was found that similar pattern for all flow rates investigated, the result of only 15 L/min simulation is presented. The average velocity values varied along the axial length of the nasal passage. This can be attributed to the change of cross section area along the nasal passage. Plug-flow model and pull-flow case study exhibited differences in the velocity profile. The nasal vestibule and the narrow constrict called the nasal valve showed major variations with respect to velocity profile between plug and pull flow boundary.

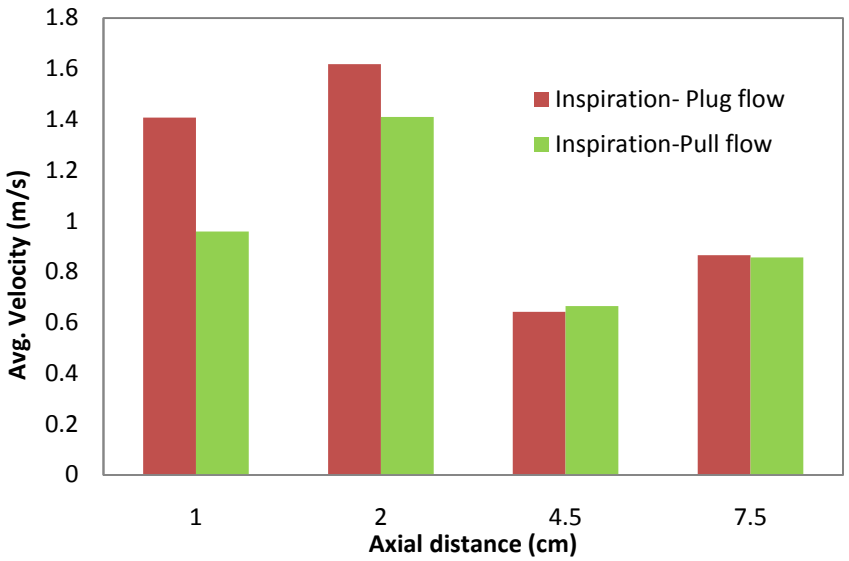

Figure 4.33: Velocity plot along the axial distance (at 15 L/min).

The average velocity for nasal vestibule and nasal valve is 1.4 m/s and 1.6 m/s for plug flow. Whereas, for pull flow case, the average velocity value in nasal vestibule and nasal valve region was observed to be around 0.96 m/s and 1.41 m/s respectively.

Beyond the nasal valve region, the boundary conditions did not have significant effect on the velocity patterns. Also it was found that the velocity distribution during expiration phase did not show much variation between pull-flow and plug-flow case. The contour plot as shown in Figure 4.34A and 4.34B shows the difference in flow patterns for both the pull flow and plug flow boundary definitions.

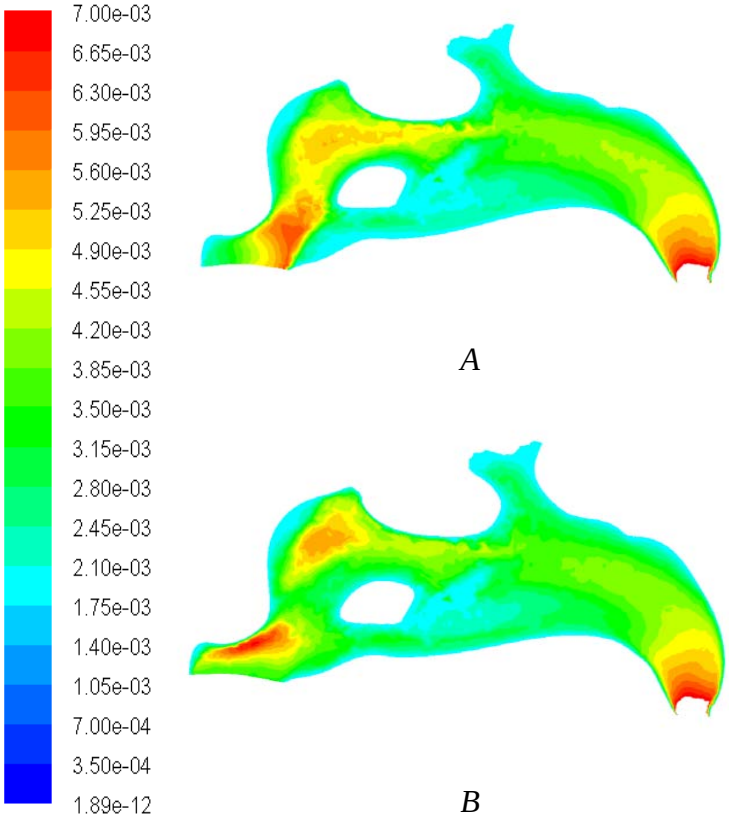

Figure 4.34: Velocity profile for pull flow A) and plug flow B) boundary condition.

4.9.3 Pressure

The major effect of using plug-flow and pull-flow boundary was with respect to the pressure distribution inside the nasal cavity. As seen in Figure 4.35A, the pressure value decreased significantly for pull flow in case of inspiration. An initial high for pressure is obtained for plug flow. This is because, in case of plug flow, a certain mass of air is forced through the nostril inlet resulting in the positive pressure value at the inlet section of the nasal cavity. This is an artifact when using plug flow boundary. The pull flow demonstrates much higher negative pressure when compared to the plug flow. This is due to the fact that, flow is sucked into the nasopharynx from the ambient atmosphere in case of pull flow which explains the much lower values of pressure in the posterior region.

Similar observation can be seen in Figure 4.35B for the expiration phase. The differences so obtained for plug-flow and pull-flow in both inspiration and expiration phases demonstrate the importance of using correct boundary conditions while modelling flow through the nasal cavity. Most of the researchers employ plug flow boundary definitions to address the flow problems associated with nasal flow. This study has revealed the fallacy of such a definition and found significant differences in values obtained in either case.

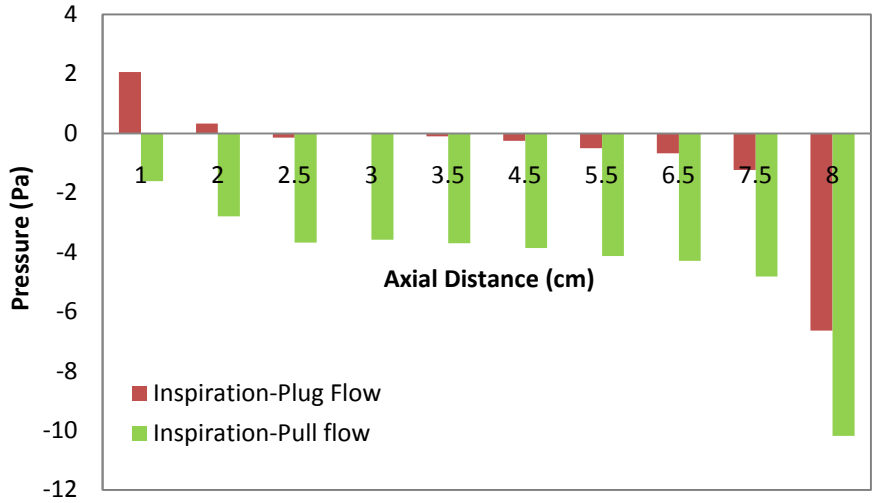

A

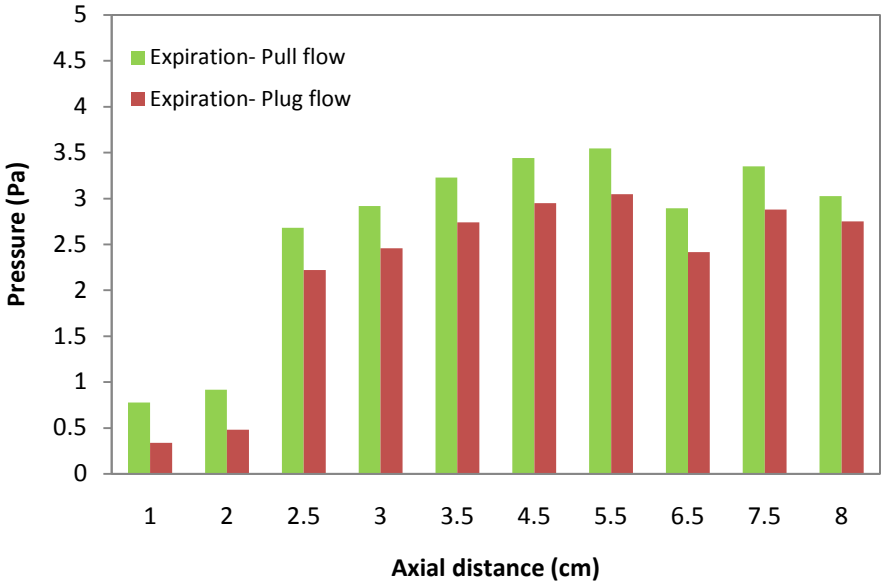

B

Figure 4.35: Pressure plot for plug and pull flow boundary condition during A) Inspiration B) Expiration.

4.9.4 Wall Shear Stress

Also, the values of wall shear stress showed differences for plug-flow and pull-flow model as seen in Figure 4.36. The plug flow boundary condition produced higher

values of stress compared to pull flow further complimenting the need for using pull-flow as boundary definition in all future references to modelling nasal airflow. Therefore, in order to quantify the results of nasal flow using numerical methods, pull flow boundary conditions must be applied. Since pull flow replicates the realistic breathing phenomenon, the results obtained using plug flow definitions are not the actual results.

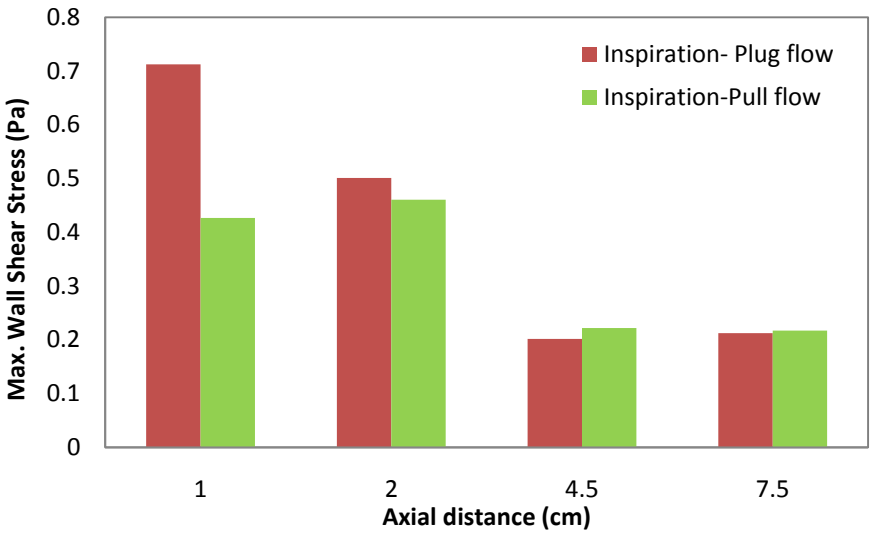

Figure 4.36: Maximum wall shear stress values during inspiration.

CHAPTER 5

CONCLUSION

5.1 Introduction

Three dimensional computational model of female human nasal cavity were developed based on the CT scans of Malaysian female subjects. Numerical simulation of inspiratory and expiratory airflow was performed for flow rates of 7.5, 10, 15, 20, 30, and 40 L/min using the developed models. This work on nasal flow study utilized female nasal cavity models as against the male models used by previous researchers. Numerical study carried on the female models has been validated with that of the male models from the data available in the literature as described in section 4.4. The effect of gender based anatomical differences on the flow behaviour also has been investigated. The effect of gravity due to change of posture is also studied. Plug flow and pull flow boundary conditions are evaluated and its effect on the nasal flow are also analyzed. In this chapter, major results, limitations of present work, and recommendation for future study are discussed.

5.2 Major conclusions drawn from this study

The following conclusions are presented based on each study topic.

5.2.1 Basic airflow studies

The flow was observed to be fully developed along the middle meatus region while the superior and inferior meatus pathway received lesser flow. This finding was consistent with that of the previous researchers (Hahn et al., 1993; Segal et al., 2008). There was sudden increase of average velocity value at the nasopharynx region which could be attributed to the decrease in cross section area at the posterior region of the nasal geometry. The nasal valve which is located at a distance of around 2 cm from the anterior region of the nasal cavity, attained the maximum velocity at around 4.18 m/s as against 4.82 m/s & 3.1 m/s obtained by Xiong *et al*., (2008) and Croce *et al*., (2006) respectively. The peak airspeed in each plane decreases posteriorly beyond nasal valve region as the cross sectional area increase. The average static pressure value decreases posteriorly along the nasal cavity. At the nasal valve where there is sudden increase in velocity due to its narrow cross- sectional area, resulted in the prevalence of higher wall shear stresses. The geometry of the septum also offered resistance to flow at the wall surface and results in the increased wall shear stresses. The flow changes direction at the nasopharynx due to the bend and this resulted in increase in wall shear stress at the posterior end. The low velocity re-circulating stream was found just posterior to the nasal valve region. This low velocity recirculatory flow at the olfactory region stimulates the olfactory nerves which is responsible for our sense of smell.

It can therefore be concluded that, the complicated anatomy of the nasal cavity has been designed to attain the physiological function desired for normal breathing. It is this structure that makes possible the sense of smell and conditioning of inspired air.

5.2.2 Various breathing rates for inspiration and expiration

Humans exhibit different breathing rate under different conditions. Irrespective of the flow rates, the highest value of average velocity appears at the nasal valve region during inspiration. Olfactory region received only a small percentage of the total flow that entered the nasal cavity. The perception of smell was improved with increased flow rates. The value of maximum wall shear stress at the vestibule region increased by more than 2000 % as the flow rate increased from 7.5 to 40 L/min. Such an abrupt increase has significant impact on blood vessels in the region. The value of maximum wall shear stress at the vestibule was around 2.92 Pa when compared to 6.89 Pa for the same location during inspiration. Therefore the sneezing phenomenon, which is characterized by abrupt and very high expiratory flow rates of greater than 40 L/min, will produce significantly lower wall shear stresses than for the same flow rate during inspiration. Hence even though sneezing is a sudden jet of flow with high velocity, the stresses produced will be much lesser. However, higher flow rates are not desired, since they result in very high values of pressure gradients which may result in the collapse of the nasal vestibule as well induce more stresses in the nasal cavity thereby damaging the delicate tissue layers and blood vessels creating complications.

5.2.3 Gravity effect on nasal airflow due to the change of posture

From the literature review it was established that the change of posture significantly affects the breathing patterns (Beaumont et al., 1998; Hsing-won Wang, 2002; Matsuzawa et al., 1995; Tvinnereim et al., 1996). Hence the gravity effect due to

the change of posture significantly influences the flow parameters and cannot be neglected. These findings hold significant importance in the study of numerical analysis of flow through the nasal cavity. The 3D model for developing the nasal cavity is obtained either from the MRI or the CT scans. Hence the numerical modelling associated with posture dynamics comes into effect. Therefore while applying the boundary conditions in the study of nasal flow using CFD; we must take into account the effect of posture and gravity. As per our knowledge none of the previous studies on numerical flow analysis take into account the effect of posture and gravity. Therefore in order to accurately predict the flow features inside the nasal airway path, we must specify the correct posture and apply appropriate boundary conditions. This study on effect of gender and posture can be considered as the major step towards standardisation of modelling approach in the domain of nasal flow studies.

5.2.4 Effect of different boundary condition on flow parameters

A 3D computational study of inspiratory airflow using plug and pull flow boundary conditions was carried out. Comparative analysis of plug flow and pull flow boundary conditions showed significant variations for various flow parameters like velocity and pressure distribution. Velocity at the vestibule and the nasal valve region was higher for plug flow when compared with pull flow. There was a very significant difference in the pressure distribution across the nasal cavity. Considerable variation was observed for resistance across the nasal cavity for pull flow and plug flow cases. The flow patterns obtained during either case were different. Hence, in order to account for the natural physiological breathing conditions, it is very important to include the correct boundary

condition. Since pull flow accounts for the natural physiological boundary definition, future research should incorporate pull-flow boundary in order to study the physiology of the nasal cavity. Based on the study, it can be concluded that difference in boundary condition will result in variation in flow behavior inside the nasal cavity. In the absence of standardization of modelling of flow through the nasal cavity, and lack of unanimity among the researchers on the type of boundary conditions to be applied, this study holds significant importance.

5.3 Future works

Based on the presented research findings, several recommendations can be drawn to facilitate and provide future direction of research works. First, higher quality of CT scan images with better pixel resolution and smaller number of increment between slice of image are need to capture accurately the nasal cavity. Highly quality of CT scan images will help reduce the time required to build the complex geometry of the nasal cavity and avoid the creation of ‘stair-step’ surface contour which will affect the airflow characteristic.

In order to capture the exact physiological nasal breathing, modelling the collapsibility of the nasal vestibule region during inspiration can be considered as a vital step. However, the inclusion of this work in the current research study which demands the study of fluid structure interaction is not possible due to the complicated structure of the nasal cavity and time constraint.

The implication of the study on posture holds importance in the future study of medicine delivery through the nasal cavity. It would be interesting to understand the

relationship in arriving at the appropriate posture for the delivery of medicine and the effectiveness of this posture for the drugs to reach the desired locations inside the nasal cavity. The study of gender effect on the nasal airflow in the future research work may also include the age and body size variation which also can be the contributing factors that affecting the nasal patency.

Further study may also be carried out to study the posture effect on nasal breathing by simulating the nasal model which developed based on the CT scan images obtained according to sitting, supine, prone and right recumbency position. Study of nasal abnormality can also be performed in order to assist ENT surgeon in pre-diagnosis of the nasal disease and plan for the treatment planning of nasal surgeries.

REFERENCES

Ahmad KA, Abdullah MZ, Watterson JK. 2010. Numerical modelling of a pitching airfoil. Jurnal Mekanikal. 30: 37-47.

Austin CE, Foreman JC. 1994. Acoustic rhinometry compared with posterior rhinomanometry in the measurement of histamine- and bradykinin-induced changes in nasal airway patency. Br J clin Pharmac. 37: 33-37.

Bailie N, Hanna B, Watterson J, Gallagher G. 2006. An overview of numerical modeling of nasal airflow. Rhinology 44(1): 53-57.

Beaumont M, Fodil R, Isabey D, Lofaso F, Touchard D, Harf A, Louis B. 1998. Gravity effects on upper airway area and lung volumes during parabolic flight. J Appl Physiol. 84: 1639-1645.

Cheng YS, Yeh HC, Guilmette RA, Simpson SQ, Cheng KH, Swift DL. 1996. Nasal deposition of ultrafine particles in human volunteers and its relationship to airway geometry. Aerosol Sci Technol. 25(3): 274-291.

Corey JP. 2006. Acoustic rhinometry: should we be using it? Current opinion in otolaryngology & head and neck surgery. 14(1): 29-34.

Croce C, Fodil R, Durand M, Sbirlea-Apiou G, Papon JF, Blondeau JR, Coste A, Isabey D, Louis B. 2006. In vitro experiments and numerical simulations of airflow in realistic nasal airway geometry. Annals of Biomedical Engineering, 34(6): 997-1007.

Devyani L, Corey JP. 2004. Acoustic rhinometry and its uses in rhinology and diagnosis of nasal obstruction. Facial plastic surgery clinics of North America. 12(4): 397-405.

Ecckes R. 1998. The relationship between subjective & objective measures of nasal function. Jpn J. Rhinol. 37: 61-69.

Elad D, Liebenthal R, Wenig BL, Einav S. 1993. Analysis of airflow patterns in the human nose. Med & Biol Eng & Comput. 31: 585-592.

Elad D, Wolf M, Keck T. 2008. Air conditioning in the human nasal cavity. Respiratory Physiology & Neurobiology. 163: 121-127.

FLUENT 6.1, User guide

Garcia GJM, Bailie N, Martin DA, Kimbell JS. 2007. Atrophic rhinitis: a CFD study of air conditioning in the nasal cavity. J Appl Physiol. 103: 1082-1092.

Hahn I, Scherer PW, and Mozell MM. 1993. Velocity Profiles Measured for Airflow Through a Large Scale Model of the Human Nasal Cavity. J Appl Physiol. 75(5): 2273-2287.

Haight JSJ, Cole P. 1983. The site and function of the nasal valve. Laryngoscope. 93: 49-55.

Hilberg O, Jackson AC, Swift DL, Pedersen OF. 1989. Acoustic rhinometry: evaluation of the nasal cavity by acoustic rhinometry. J Appl Physiol. 66: 295-303.

Hsing-won Wang. 2002. Effects of posture on nasal resistance. J Med Sci. 22(4): 161-164.

Inthavong K, Wen J, Tian ZF, Tu J. 2007. Numerical study of fibre deposition in a human nasal cavity. Aerosol science. 39: 253-265.

Ishikawa S, Nakayama T, Watanabe M, Matsuzawa T. 2009. Flow mechanisms in the human olfactory groove. Arch Otolaryngol Head Neck Surg. 135(2): 156-162.

Jones AS and Lancer M. 1987. Rhinomanometry. Clin Otolaryngol. 12: 233-236.

Kenyon GS. 1987. Phase variation in nasal airway resistance as assessed by active anterior rhinomanometry. Journal of Laryngology and Otology. 101: 910-916.

Keyhani K, Scherer PW, Mozell MM. 1995. Numerical simulation of airflow in the human nasal cavity. J. Biomech. Eng. 117: 429–441.

Kjærgaard T, Cvancarova M, Steinsvag SK. 2009. Relation of nasal air flow to nasal cavity dimensions. Arch Otolaryngol Head Neck Surg. 135(6): 565-570.

Lindemann J, Brambs HJ , Keck T, Wiesmiller KM, Rettinger G, Pless D. 2005. Numerical simulation of intranasal airflow after radical sinus surgery. American Journal of Otalarynology-Head and Neck Medicine & Surgery. 26: 175-180.

Liu Y, Matida EA, Gu J, Johnson MR. 2007. Numerical simulation in a 3-D human nasal cavity using RANS, RANS/EIM, and LES. Aerosol Sciences. 38: 683-700.

Mamikoglu B, Houser S, Akbar I, Ng B, Corey J P. 2000. Acoustic rhinometry and computed tomography scans for the diagnosis of nasal septal deviation, with clinical correlation. Otolaryngology--head and neck surgery : official journal of American Academy of Otolaryngology-Head and Neck Surgery 123(1 Pt 1): 61-8.

Martin SE, Mathur R, Marshall I, Douglas NJ. 1997. The effect of age, sex, obesity and posture on upper airway size. Eur Respir J. 10: 2087-2090.

Matsuzawa Y, Hayashi S, Yamaguchi S, Yoshikawa S, Okada K, Fujimoto K, Sekiguchi M. 1995. Effect of prone position on apnea severity in obstructive sleep apnea. Internal Medicine. 34(12): 1190-1193.

Min YG, Jang YJ. 1995. Measurements of cross-sectional area of the nasal cavity by acoustic rhinometry and CT scanning. Laryngoscope. 105(7 Pt 1): 757-759

Mohsenin V. 2003. Effects of gender on upper airway collapsibility and severity of obstructive sleep apnea. Sleep Medicine. 4: 523–529.

Mullins LJ. 1944. Olfaction. Ann NY Acad Sci. 62: 247-276.

Mylavarapu G, Murugappan S, Mihaescu M, Kalra M, Khosla S, Gutmark E. 2009. Validation of computational fluid dynamics methodology used for human upper airway flow simulations. J Biomech. 42: 1553-1559.

Naftali S, Schroter RC, Shiner RJ, Elad D. 1998. Transport phenomena in the human nasal cavity: a computational model. Ann. Biomed. Eng. 26: 831–839.

Oksenberg A, Silverberg DS. 1998. The effect of body posture on sleep-related breathing disorders: facts and therapeutic implications. Sleep Medicine Reviews. 2(3): 139-162.

Probst R, Grevers G, Iro H. 2006. Basic Otorhinolaryngology: A step-by-step learning guide. New York: Thieme. P.3.

Proctor DF, Andersen IB.1982. The nose: upper physiology and the atmospheric environment. New York: Elsevier Biomedical Press.P.30.

Reber M, Rahm F. and Monnier P. 1998. The role of acoustic rhinometry in the pre- and postoperative evaluation of results for nasal obstruction, *Rhinology*. 36(4): 184–187.

Riechelmann H, O'Connell JM, Rheinheimer MC, Wolfensberger M, Mann WJ. 1999. The role of acoustic rhinometry in the diagnosis of adenoidal hypertrophy in pre-school children. Eur J Pediatr. 158(1): 38-41.

Roithmann R, Demeneghi P, Faggiano R, Cury A. 2005. Effect of posture change on nasal patency. Rev Bras Otorrinolaringol. 71(4): 478-84.

Rowley JA, Zhou X, Vergine I, Mahdi A, Shkoukani, Badr MS. 2001. Influence of gender on upper airway mechanics: upper airway resistance and Pcrit. J Appl Physiol. 91: 2248-2254.

Schneider R, Costiole JP, Vega A, Wolf S. 1963. Olfactory threshold technique with nitrogen dilution of n-butane and gas chromatography. J Appl Physiol. 18:414-417.

Segal RA, Kepler GM, Kimbell JS. 2008. Effects of differences in nasal anatomy on airflow distribution: a comparison of four individuals at rest. Ann Biomed Eng. 36 (11):1870-1882.

Shelton DM, Eiser NM. 1992. Evaluation of anterior and posterior rhinomanometry in normal subject. Clin Otolaryngol Allied Sci. 17(2): 178-82.

Sipila J, Suonpaa J. 1997. A prospective study using rhinomanometry and patient clinical satisfaction to determine if objective measurements of nasal airway resistance can improve the quality of septoplasty. Eur Arch Otorhinolaryngol. 254: 387-90.

Subramaniam RP, Richardson RB, Morgan KT, Kimbell JS, Guilmette RA. 1998. Computational fluid dynamics simulations of inspiratory airflow in the human nose and nasopharynx. Inhal. Toxicol. 10: 91–120.

Suzina AH, Hamzah M, Samsudin AR. 2003. Active anterior rhinomanometry analysis in normal adult Malays. The Journal of laryngology and otology. 117(8): 605-8.

Thurnheer R, Wraith PK, Douglas NJ. 2001. Influence of age and gender on upper airway resistance in NREM and REm sleep. J Appl Physiol. 90: 981-988.

Tomkinson A & Eceles R. 1995. Errors arising in cross sectional area estimation by acoustic rhinometry produced by breathing during measurement. Rhinology 33: 138-140.

Tomkinson A & Eceles R. 1998. Acoustic rhinometry: an explanation of some common artifacts associated with nasal decongestants. Clin Otolaryngol 23: 20-26.

Tvinnereim M, Cole P, Mateika S, Haight J, Hoffstein V. 1996. Postural changes in respiratory airflow pressure and resistance in nasal, hypopharyngeal, and pharyngeal airway in normal subjects. The Annals of otology, rhinology and laryngology. 105(3): 218-221.

Viani L, Jones AS, Clarke R. 1990. Nasal airflow in inspiration and expiration. Journal of Laryngology and Otology. 104: 473-476.

Watanabe T, Isono S, Tanaka A, Tanzawa H, Nishino T. 2002. Contribution of body habitus and craniofacial characteristics to segmental closing pressures of passive pharynx in patients with sleep disordered breathing. Am J Respir Crit Care Med. 165:260–265.

Weinhold I, Mlynski G, 2004. Numerical simulation of airflow in the human nose. Eur Arch Otorhinolaryngol. 261: 452-455.

Wen J, Inthavong K, Tu J, Wang S. 2008. Numerical simulations for detailed airflow dynamics in a human nasal cavity. Respir Physiol Neuro. 161: 125–135.

Wexler D, Segal R, Kimbell J. 2005. Aerodynamic Effects of Inferior Turbinate Reduction computational Fluid Dynamics Simulation. Arch Otolaryngol Head Neck Surg. 131: 1102-1107.

Xiong GX, Zhan JM, Jiang HY, Li JF, Rong LW, Xu G.2008. Computational fluid dynamics simulation of airflow in the normal nasal cavity and paranasal sinuses. Am J Rhinol. 22: 477-82.

Zamankhan P, Ahmadi, Wang ZC. 2006. Airflow and deposition of nanoparticles in a human nasal cavity. Aerosol Sci. Technol. 40: 463–476.

Zhao K, Dalton P, Yang GC, Scherer PW. 2006. Numerical modelling of turbulent and laminar airflow and odorant sniffing in the human and rat nose. Chem Senses. 31: 107-118.

Zubair M, Vizy RN, Abdullah MZ, Ismail R, Shuaib IL, Suzina AH, Ahmad KA. 2010. Airflow inside the nasal cavity: visualization using computational fluid dynamics. Asian Biomedicine. 4: 657-661.

LIST OF PUBLICATIONS

1. Zubair M, Vizy RN, Abdullah MZ, Ismail R, Shuaib IL, Suzina AH, Ahmad KA. 2010. Airflow inside the nasal cavity: visualization using computational fluid dynamics. Asian Biomedicine. 4: 657-661.

2. Vizy RN, Zubair M, Abdullah MZ, Ismail R, Shuaib IL, Suzina AH, Ahmad KA. 2010. Numerical Study of Inspiratory and Expiratory Flow in a Human Nasal Cavity. Journal of medical and biological engineering. Journal of Medical and Biological Engineering.31(3):201-206.

3. Vizy RN, Zubair M, Abdullah MZ, Ismail R, Shuaib IL, Suzina AH, Ahmad KA. 2010. Boundary condition prescription for nasal airflow studies using numerical method. (Under review)

4. Vizy RN, Zubair M, Abdullah MZ, Ismail R, Shuaib IL, Suzina AH, Ahmad KA. 2010. Numerical study on the effect of gender and posture on the airflow characteristics inside the nasal cavity. (Under review)

REFEREED CONFERENCE PAPERS

1. Vizy RN, Zubair M, Abdullah MZ, Ismail R, Shuaib IL, Suzina AH, Ahmad KA. Numerical study of the nasal resistance and flow features inside the nasal cavity using the pull-flow. World Engineering Congress 2010, 2^{nd}–5^{th} August 2010, Kuching, Sarawak, Malaysia.

2. Vizy RN, Zubair M, Abdullah MZ, Ismail R, Shuaib IL, Suzina AH, Ahmad KA. Numerical simulation of airflow in a 3d model of human nasal cavity. 1ST Mechanical & Aerospace Engineering Research Colloquium 2010 9^{th}-10^{th} June 2010, School of Mechanical Engineering, Universiti Sains Malaysia.

3. Zubair M, Vizy RN, Abdullah MZ, Ismail R, Shuaib IL, Suzina AH, Ahmad KA. Use of Numerical Methods in determining the airflow dynamics and impedance within the nasal cavity. World Engineering Congress 2010, 2^{nd}–5^{th} August 2010, Kuching, Sarawak, Malaysia.

4. Zubair M, Vizy RN, Abdullah MZ, Ismail R, Shuaib IL, Suzina AH, Ahmad KA. Virtual surgery of the nasal cavity – review. 1ST Mechanical & Aerospace Engineering Research Colloquium 2010 9^{th}–10^{th} June 2010, School of Mechanical Engineering, Universiti Sains Malaysia.